The neonatal gut microbiota: a role in the encephalopathy of prematurity

Authors and affiliations

Kadi Vaher[a,b], Manuel Blesa Cabez[a,b], Paula Lusarreta Parga[c], Justyna Binkowska[c], Gina J van Beveren[d], Mari-Lee Odendaal[e], Gemma Sullivan[a,b], David Q Stoye[a], Amy Corrigan[a], Alan J Quigley[f], Michael J Thrippleton[b], Mark E Bastin[b], Debby Bogaert[c,d,#], and James P Boardman[a,b,#*]

[a]MRC Centre for Reproductive Health, Institute of Regeneration and Repair, University of Edinburgh, Edinburgh, United Kingdom

[b]Centre for Clinical Brain Sciences, University of Edinburgh, Edinburgh, United Kingdom

[c]Centre for Inflammation Research, Institute of Regeneration and Repair, University of Edinburgh, Edinburgh, United Kingdom

[d]Department of Pediatric Immunology and Infectious Diseases, Wilhelmina Children's Hospital and University Medical Center Utrecht, Utrecht, the Netherlands

[e]Centre for Infectious Disease Control, National Institute for Public Health and the Environment, Bilthoven, The Netherlands

[f]Department of Paediatric Radiology, Royal Hospital for Children and Young People, Edinburgh, United Kingdom

[#]DB and JPB contributed equally to the work

***Corresponding author**: James P Boardman, Queen's Medical Research Institute, 47 Little France Crescent, Edinburgh EH16 4TJ, UK. Email: James.Boardman@ed.ac.uk

Abstract

Preterm birth is associated with atypical brain development and alterations in the gut microbiome. Variation in gut microbiome composition associates with neurobehavioural outcomes, but its relationship with brain development in preterm infants is unknown. First, we characterised the faecal microbiome in an observational cohort of 135 preterm (<32 weeks' gestation) and 12 term neonates using 16S-based and shotgun metagenomic sequencing. Apart from sampling age, delivery mode had the strongest association with preterm microbiome shortly after birth; low birth gestational age, infant sex and antibiotics significantly associated with microbiome composition at NICU discharge. Second, we integrated these data with structural and diffusion MRI at term-equivalent age. Bacterial community composition associated with MRI features of encephalopathy of prematurity. Particularly, abundances of *Escherichia coli* and *Klebsiella* spp. correlated with microstructural parameters in deep and cortical grey matter. Metagenome functional capacity analyses using gut-brain modules suggested that these bacteria interact with brain microstructural development via tryptophan and propionate metabolism. This study indicates a role for microbiota-brain interactions in brain development following preterm birth.

Keywords: preterm, neonate, brain MRI, gut microbiome, encephalopathy of prematurity

Introduction

Globally, preterm birth, defined as birth before 37 weeks of gestation, affects around 10% of pregnancies[1]. People born preterm are at an increased risk for atypical brain development, termed encephalopathy of prematurity (EoP)[2], which can lead to cerebral palsy, neurodevelopmental and cognitive impairments, autism, and psychiatric disorders[3]. There are no treatments for EoP, partly because the mechanisms linking preterm birth with altered cerebral development are incompletely understood.

The second and third trimesters of pregnancy are crucial periods in brain development. During this time, preterm birth and its co-exposures and -morbidities impose a risk of injury and dysmaturation to the developing brain, leading to disturbances in regional brain growth, diffuse white matter disease, abnormal cortical and deep grey matter (dGM) development, and structural dysconnectivity[4]. These features of EoP are apparent on structural and diffusion magnetic resonance imaging (MRI) in the neonatal period[4] and, because they are associated with subsequent neurocognitive development[5–8], they serve as intermediate phenotypes to investigate the upstream determinants of brain development.

Fundamental neurodevelopmental processes occurring in early life coincide with the acquisition and progression of the gut microbiota. Evidence from preclinical and human observational studies implicates the gut microbiome in modulating neural functions via the microbiota-gut-brain axis[9,10]. Specifically, the rapid parallel development of the brain and the gut microbiota in early life has led to the hypothesis of 'nested sensitive periods' whereby brain development interacts with gut microbiota development to shape cognition and behaviour[11,12]. The theory has gained traction from a growing body of literature reporting associations between gut microbiota features and cognitive, language, motor, and socio-emotional development in childhood[13].

Preterm infants may be particularly vulnerable to disruptions in the microbiota-gut-brain axis due to altered microbiota development, which can arise from the early exposure of the immature gastrointestinal tract to microbial colonisation[14,15]. Although the general pattern of microbiota development in the first months of life appears similar in term and preterm infants[16–18], the preterm infant gut has lower bacterial diversity and abundances of essential microbes like *Bifidobacterium*, and higher levels of opportunistic pathogens such as *Klebsiella, Enterobacter, Enterococcus* and *Staphylococcus*[14]. This may be a result of routine but unavoidable exposure to potent modifiers of the pioneering microbiota, including maternal and neonatal antibiotic treatments[19], and variable nutritional exposures[20,21] during the first months of life in a neonatal intensive care unit (NICU) setting. However, there are discrepancies between studies about the effect size and direction of these modifiers in preterm neonates[22], which leaves considerable uncertainty about the importance of specific clinical variables for shaping microbiota development following preterm birth.

Although the preterm population has a high burden of neurocognitive impairment and alterations in the gut microbiota, only a few recent studies have investigated gut microbiota in direct relation to preterm infant neurodevelopment[23–27] or overt parenchymal brain injuries[28]. Though most of these studies have been small and directions of effects vary, there is some consensus that abundances of *Bifidobacteriaceae*, *Enterococcaceae, Enterobacteriaceae* (*Escherichia/Shigella, Enterobacter, Klebsiella*), *Clostridium,* and *Veillonella* may correlate with outcomes. However, to our knowledge, no studies have investigated the preterm microbiota in association with EoP. This question is important because EoP is the prevailing form of brain dysmaturation after preterm birth and the gut microbiota is intrinsically modifiable by mode of feeding and enteral supplements, which offer potential new avenues for perinatal neuroprotection.

We investigated the microbiota-gut-brain axis by integrating data from microbiota profiling and multimodal brain MRI. We aimed to characterise neonatal gut microbiota profiles in a richly-phenotyped cohort of term and preterm neonates at birth and at NICU discharge; to determine the most influential clinical drivers of the preterm microbiota during NICU care; and to link gut microbiota diversity and community composition with MRI features of EoP.

Results

Sample characteristics

The gut microbiome was sampled at two timepoints (TP1: meconium, and TP2: a faecal sample prior to discharge from NICU) in very preterm infants born < 32 completed weeks of gestation, and at TP1 in term-born controls, who were recruited to the Theirworld Edinburgh Birth Cohort (TEBC)[29]. Clinical and demographic characteristics of the study group are shown in Table 1; see Supplementary Fig. 1 for flowchart.

Table 1 Baseline characteristics of the study group.

Variable*	level	Full-term	Preterm	p-value$ (term vs preterm)	Preterm with matching MRI
Sample size		12	135		79
GA at birth, weeks (median [range])		40.00 [37.71, 42.00]	29.14 [22.14, 32.86]	<0.001	29.86 [22.14, 32.86]
Timepoint 1: number of samples		12	58		
Timepoint 1: postnatal age, days (median [range])		1 [1, 3]	6 [1, 13]	<0.001	/
Timepoint 1: GA, weeks (median [range])		40.14 [37.86, 42.00]	29.14 [24.43, 33.57]	<0.001	/
Timepoint 2: number of samples		/	103		79
Timepoint 2: postnatal age, days (median [range])		/	46 [9, 151]		45 [9, 151]
Timepoint 2: GA, weeks (median [range])		/	36.14 [29.43, 46.14]		35.85 [32.43, 46.14]
Female infants (%)		9 (75.0)	64 (47.4)	0.078	36 (45.6)
Birthweight, g (mean (SD))		3530 [2740, 4420]	1190 [370, 2510]	<0.001	1282 [370, 2510]
Birthweight z-score (median [range])		0.843 [-0.818, 2.331]	0.212 [-3.023, 2.141]	0.011	0.153 [-2.520, 2.141]
GA at MRI, weeks (mean (SD))		/	/		40.56 (1.8)
Weeks between faecal sample collection and MRI (mean (SD))		/	/		3.81 (2.65)
Vaginal delivery (%)		11 (91.7)	41 (30.4)	<0.001	21 (26.6)
Antenatal steroids given (%)		/	128 (94.8)		74 (93.7)
Magnesium sulphate given (%)		/	104 (77.0)		54 (68.4)
Labour antibiotics (%)		1 (8.3)	89 (65.9)	<0.001	48 (60.8)
Membrane rupture duration, hours (median [range])		10 [0, 63]	0 [0, 1043]	0.132	0 [0, 934]
Days in NICU (median [range])		/	61 [6, 167]		60 [17, 167]
Bronchopulmonary dysplasia (%)		/	41 (30.4)		24 (30.4)
Necrotising enterocolitis (%)		/	7 (5.2)		3 (3.8)
Sepsis (%)		/	41 (30.4)		19 (24.1)
Retinopathy of prematurity (%)		/	9 (6.7)		5 (6.3)

Antibiotics <72h of life (%)		/	106 (78.5)		62 (78.5)
Antibiotics >72h of life (%)		/	77 (57.0)		38 (48.1)
Total days of antibiotics during NICU stay (median [range])		/	4 [0, 49]		3 [0, 47]
Proportion of days receiving antibiotics during NICU stay (median [range])		/	0.094 [0.000, 0.843]		0.091 [0.000, 0.708]
GA at discharge (median [range])		/	37.57 [30.57, 48.43]		37.43 [34.43, 48.43]
Breastmilk exposure	<75% inpatient days	/	73 (54.1)		43 (54.4)
	≥75% inpatient days	/	62 (45.9)		36 (45.6)
Proportion of days receiving exclusive breastmilk during NICU stay (median [range])		/	0.686 [0.000, 1.000]		0.663 [0.000, 1.000]
Proportion of days receiving exclusive formula during NICU stay (median [range])		/	0.000 [0.000, 0.895]		0.000 [0.000, 0.895]
Proportion of days receiving mixed feeds during NICU stay (median [range])		/	0.098 [0.000, 0.962]		0.092 [0.000, 0.962]
Feeding at discharge (%)	Breastfeeding	12 (100.0)	51 (37.8)		32 (40.5)
	Formula feeding	0 (0.0)	43 (31.9)		18 (22.8)
	Mixed feeding	0 (0.0)	41 (30.4)		29 (36.7)
Maternal age, years (mean (SD))		33 (3.5)	32 (5.6)	0.401	33 (5.4)
Maternal BMI (median [range])		24.7 [20.9, 33.2]	26.7 [16.4, 46.6]	0.502	26.5 [16.4, 46.6]
SIMD rank (%)	1	0 (0.0)	31 (23.0)	0.075	17 (21.5)
	2	1 (8.3)	29 (21.5)		11 (13.9)
	3	4 (33.3)	21 (15.6)		13 (16.5)
	4	1 (8.3)	17 (12.6)		10 (12.7)
	5	6 (50.0)	37 (27.4)		28 (35.4)

**Categorical variables are shown in absolute numbers with percentages (%); continuous, normally distributed variables as means with standard deviations (SD); continuous, non-normally distributed variables as medians with ranges. $Two-sample t-tests were used to compare the means of normally distributed continuous variables between term and preterm infants; Wilcoxon rank-sum tests were applied to compare medians of non-normally distributed continuous variables; Fischer's exact test was used to test for significant differences in categorical variables. GA = gestational age; SIMD = Scottish Index of Multiple Deprivation; NICU = neonatal intensive care unit.*

Overview of microbiota profiles

We first characterised neonatal intestinal microbiome profiles using 16S ribosomal RNA (rRNA) gene sequencing in 12 term and 58 preterm infants at TP1 and in 103 preterm infants at TP2. Shotgun metagenomic sequencing data was available for 23 preterm infants at TP1 and 97 preterm infants at TP2. Throughout the paper, 16S-based data is described at amplicon sequence variant (ASV)-level, while shotgun taxonomic data is described at species-level.

The majority of TP1 samples were dominated by an ASV from the genus *Staphylococcus*, but some had high relative abundances of ASVs belonging to genera *Streptococcus*, *Escherichia/Shigella, Enterococcus,* or *Klebsiella* (Fig. 1a). Using shotgun sequencing, the most abundant species in the subset of TP1 samples were *Escherichia coli, Enterococcus faecalis, Staphylococcus epidermidis* and *S. haemolyticus,* and *Raoultella planticola* (Supplementary Fig. 2a). At TP2, most samples had high relative abundances of ASVs belonging to *Bifidobacterium, Enterobacteriaceae* or *Escherichia/Shigella,* whilst some had high relative abundances of a *Klebsiella* ASV (Fig. 1a).

Shotgun sequencing showed similar profiles, but allowed better species-level resolution, with high abundances of *Bifidobacterium* spp. (*B. breve, B. longum, B. dentium*), *E. coli, E. faecalis*, or *Klebsiella* spp. (*K. pneumoniae, K. oxytoca*; Supplementary Fig. 2a).

Collectively, we observed a marked shift in the preterm gut microbiota community composition between birth and term-equivalent age (TEA) when analysed at ASV- or species-level (permutational analysis of variance [PERMANOVA] R^2 = 14.59%, p = 9.99 × 10^{-4} [Fig. 1b]; R^2 = 3.31%, p = 002 [Supplementary Fig. 2c], respectively). Differences in the microbiota between the two timepoints were also reflected in alpha diversity (Fig. 1c; linear mixed effects model; $F_{2,112.86}$ = 47.244, q = 2.48 × 10^{-15} for Shannon index; $F_{2,151.99}$ = 22.876, q = 2.06 × 10^{-9} for observed species): both Shannon index (q = 4.00 × 10^{-14}) and number of observed species (q = 6.88 × 10^{-9}) were higher at TP2 in preterm infants. From the shotgun data, we also derived gut metabolic modules (GMM)[30,31] to capture microbiome functional capacity (Supplementary Fig. 2b depicts the most abundant GMMs present in the dataset). When comparing preterm infants at birth and at TEA, we found, similarly to taxonomic composition, a statistically significant difference between the two timepoints (PERMANOVA R^2 = 4.17%, p = 9.99 × 10^{-4}; Supplementary Fig. 2d).

Comparison of term and preterm infants at TP1 revealed a small difference in bacterial community composition at ASV-level (R^2 = 2.75%, p = 0.082; Fig. 1b). Preterm infants had higher relative abundances of ASVs belonging to *Escherichia/Shigella* (q = 0.189) and *Streptococcus* (q = 0.223) genera, while term infants had higher abundance of a *Corynebacterium* ASV (q = 0.131; Supplementary Table 1). Term infants also had a significantly higher number of observed species compared to preterm infants (q = 7.75 × 10^{-5}; Fig. 1c), whilst no differences were found in Shannon index (q = 0.571).

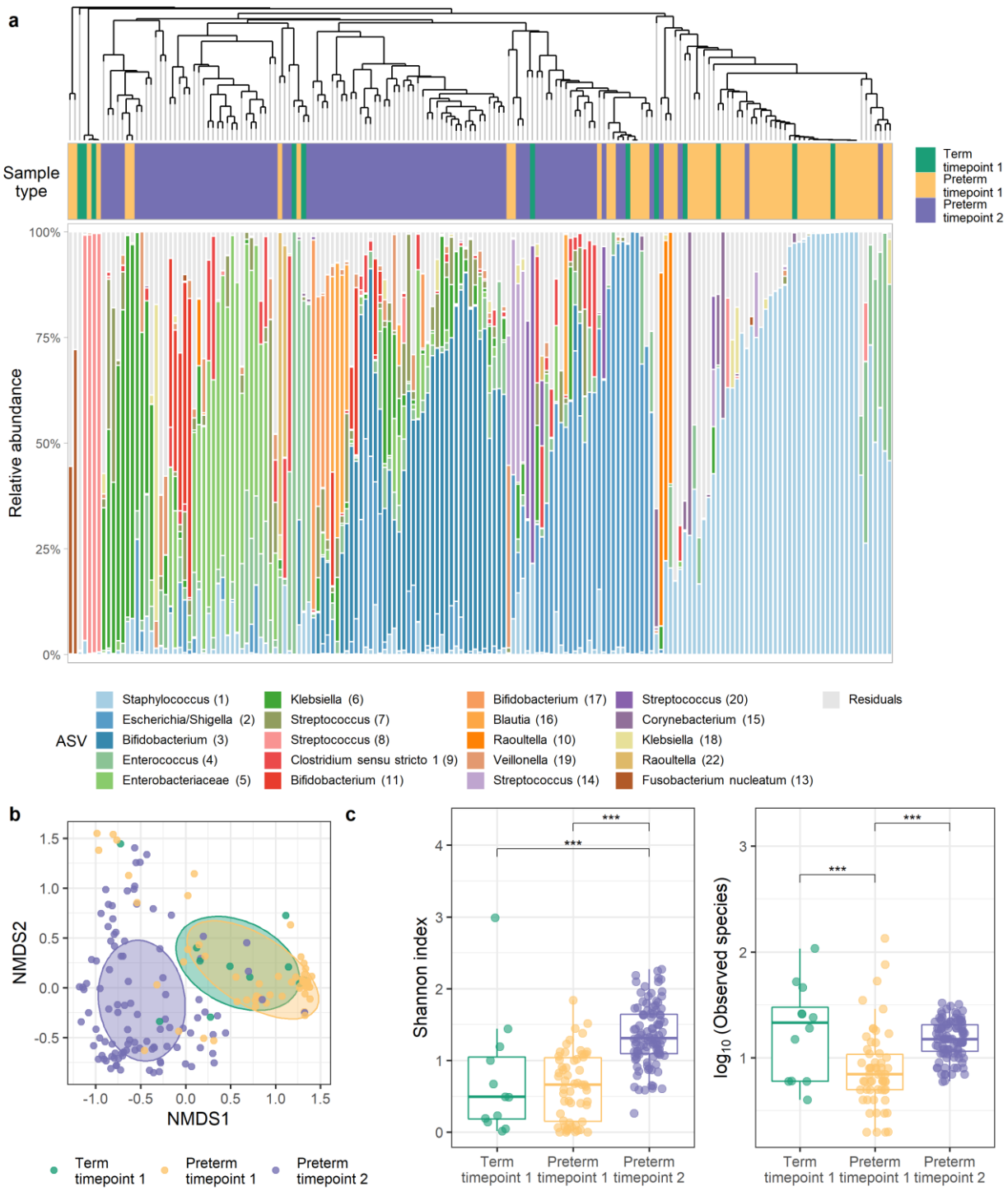

Fig. 1 Overview of microbiota profiles in neonates based on 16S rRNA gene sequencing. **a** Relative abundances of the 20 most abundant ASVs identified across the dataset are visualised per sample. Samples are ordered based on hierarchical clustering of the Bray-Curtis dissimilarity matrix using average linkage (see dendrogram). **b** Non-metric multidimensional scaling (NMDS) plot based on Bray–Curtis dissimilarity between samples; data points and ellipses are coloured by sample type. The ellipses denote the standard deviation of data points belonging to each sample type, with the centre points of the ellipses calculated using the mean of the coordinates per group. **c** Microbiota alpha diversity measured by Shannon index (left) and observed species (right). *** indicates $q < 0.001$ in pairwise comparisons using *emmeans* following linear mixed effects model comparing alpha diversity indices between the groups and timepoints. Sample sizes: term timepoint 1 = 12, preterm timepoint 1 = 58, preterm timepoint 2 = 103.

Covariates shaping preterm infant gut microbiome

We then sought to identify perinatal covariates associated with microbiota communities in preterm infants, focussing on variables known from literature to associate with microbiota composition in term infants (gestational age [GA] at birth, age at sampling, birthweight, delivery more, antibiotics, breastmilk exposure), and the most common preterm neonatal co-morbidities (sepsis, necrotising enterocolitis [NEC], bronchopulmonary dysplasia [BPD]). Although sex is not often investigated in association with early life gut microbiota development and previous studies report mixed findings to the extent that sex associates with infant microbiota[32,33], we included this variable because boys and girls differ in susceptibility to mortality and major morbidities following preterm birth[34].

In univariable models, ASV-level bacterial community composition at TP1 significantly associated with mode of delivery, birthweight z-score, and postnatal age at sample collection (Fig. 2a left panel). Using shotgun sequencing, the different perinatal factors had relatively stronger correlations with species-level community composition, though most did not remain significant after adjustment for multiple comparisons (Fig. 2 middle panel). Interestingly, delivery mode explained a smaller proportion of variance, and antibiotic treatment during labour a larger proportion of variance compared to ASV-level community composition.

At TP2, we observed the strongest associations for ASV-level bacterial community composition with the degree of prematurity, followed by postnatal age and GA at sample collection, antibiotic exposure, and sex (Fig. 2a left panel). Using shotgun sequencing, none of the tested covariates were statistically significantly associated with community composition, though ranking of the effect sizes was similar (Fig. 2a middle panel).

We then characterised the associations between the abundance of individual ASVs/species and clinical covariates in more detail using Microbiome Multivariate Association with Linear Models (MaAsLin2[35]). At baseline, we adjusted for postnatal age (TP1), or GA at birth and sample collection (TP2); in fully adjusted models, all covariates with q-value < 0.1 from univariable PERMANOVAs were tested simultaneously. Using 16S-based ASV-level data (Supplementary Tables 2-3), samples collected from vaginally-born preterm infants at TP1 contained, among others, higher abundance of *Escherichia/Shigella* (q = 0.172), whilst *Staphylococcus* was more abundant in caesarean section (C-section)-born infants (q = 0.023; Fig. 2b top panel). Birthweight z-score negatively correlated with the abundance of *Staphylococcus* (q = 0.217), but not when adjusting for delivery mode (Fig. 2b bottom panel). At TP2 (Fig. 2c), the faecal samples of extremely compared to very preterm infants had higher relative abundances of different *Veillonella* ASVs (q range 0.008 – 0.078) and *Klebsiella* (q = 0.160), and lower levels of *Staphylococcus* (q = 0.037; Fig. 2c left panel). We found that male infants had higher relative abundances of *Veillonella* (q = 0.216), *Bifidobacterium* (q = 0.171), and *Streptococcus* (q = 0.011), and antibiotic-exposed infants had higher relative abundance of *Klebsiella* (q = 0.110). The main results of the full mutually adjusted model (Fig. 2c right panel) paralleled those of the baseline model, though some relationships were no longer statistically significant. Species-level analyses from shotgun sequencing showed similar top hits to those observed with ASVs from 16S (Supplementary Tables 4-5), including the higher abundance of *Veillonella parvula* in extremely preterm infants and lower levels of *Streptococcus vestibularis* in girls at TP2. However, it also revealed additional information; for example, delivery mode and birthweight z-score associated with different *Staphylococcus* spp. at TP1.

Bacterial alpha diversity minimally correlated with the perinatal covariates (Supplementary Table 6): no significant correlations were found at TP1, whilst at TP2, bacterial richness correlated positively with age at sampling (postnatal and GA), and birthweight z-score, and it was higher in extremely compared to very preterm infants, and in infants diagnosed with NEC. In a mutually adjusted model

for these covariates, birthweight z-score remained statistically significantly associated with observed species, whilst the effect of degree of prematurity was attenuated (Supplementary Table 6).

Complementary analysis of the functional capacity of the microbiome using the GMMs (Fig. 2a right panel) revealed nominally significant associations for birthweight z-score and labour antibiotics at TP1, though these relationships did not remain significant after adjustment for multiple comparisons. At TP2, none of the covariates tested had statistically significant associations with community composition at the functional GMM level.

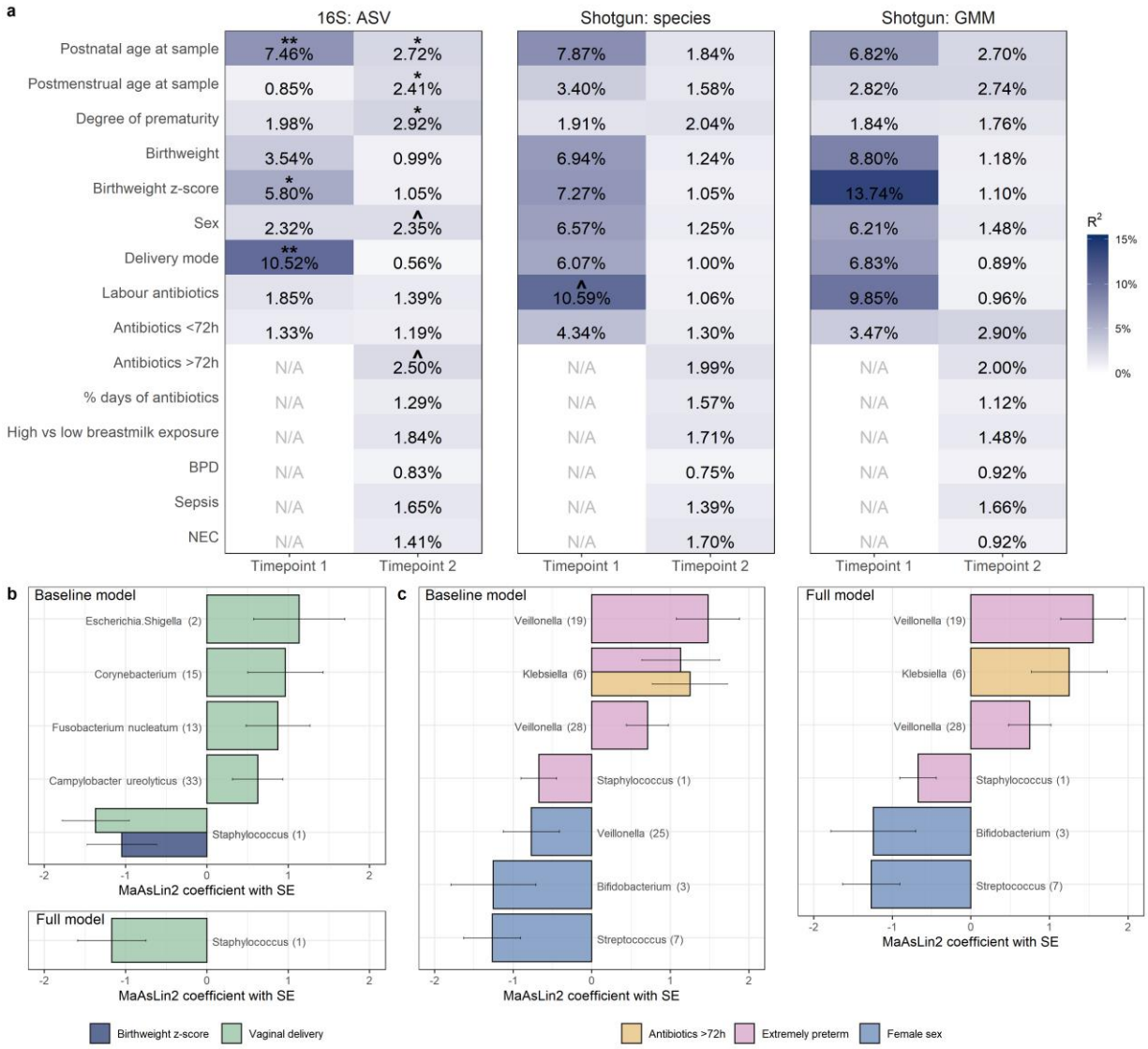

Fig. 2 Covariates associated with preterm infant gut microbiota. **a** Univariable PERMANOVA results showing the association between perinatal variables and the gut bacterial community composition at each timepoint and for each data type: left panel = ASV from 16S rRNA sequencing, middle panel = species from shotgun sequencing, right panel = Gut metabolic modules (GMM) calculated from KEGG orthologs arising from shotgun sequencing. The variance explained is estimated for each variable independently and is indicated by a percentage/blue shades. Significance of PERMANOVA was based on 1000 permutations and was adjusted for multiple comparisons using the Benjamini-Hochberg (BH) method; asterisks denote statistical significance (^$q \leq 0.1$, *$q \leq 0.05$, **$q \leq 0.01$). **b,c** Differentially abundant ASVs in association with perinatal factors at timepoint 1 (**b**) and 2 (**c**). Bar plots depict MaAsLin2-analysis results. ASVs present with at least 1% of abundance in at least 5% of samples were analysed (14 ASVs for timepoint 1 and 21 for timepoint 2) and significant results are shown (BH corrected $p < 0.25$ as default). Bars are coloured according to the covariate they are associated with. Lengths of the bars correspond with the MaAsLin2-model coefficient, which relates to the strength of the association. Error bars indicate the standard error (SE) of the model coefficient. Baseline model indicates adjustment for postnatal age at sample collection (**b**) or gestational age at birth and at sample collection (**c**). Full model indicates model where all perinatal covariates and age at sampling were analysed simultaneously. Here, GA at birth was dichotomised to group the infants into extremely (GA at birth < 28

completed weeks) and very (GA at birth < 32 completed weeks) preterm. Sample sizes for 16S rRNA sequencing: preterm timepoint 1 = 58, preterm timepoint 2 = 103; sample sizes for shotgun sequencing: preterm timepoint 1 = 23, preterm timepoint 2 = 97.

Gut microbiota associations with MRI features of encephalopathy of prematurity

Following characterisation of the preterm infant microbiota, we investigated associations between the gut microbiome and MRI biomarkers of EoP at TEA in 79 infants.

We first sought to reduce the multidimensionality of the data into a meaningful set of variables capturing the variation in the microbiota compositional data. We extracted four principal coordinates (PCo; Supplementary Fig. 3) calculated from ASV-level Bray-Curtis dissimilarity matrix; these together explained 40.9% of variance in the microbiota community composition data. Correlation analysis between the relative abundance of ASVs and the four PCo-s revealed that PCo1 mainly indicated lower relative abundances of *Bifidobacterium* and *Cutibacterium*, and, though with a weaker correlation coefficient, higher abundances of *Staphylococcus* and a set of *Enterobacteriaceae*; PCo2 indicated lower relative abundances of *Escherichia/Shigella* and higher abundances of an unidentified ASV in *Enterobacteriaceae* family*;* PCo3 mainly indicated lower abundances of *Klebsiella* and, to lesser extent, higher abundances of *Enterobacteriaceae*; and PCo4 indicated lower abundances of *Enterococcus* and interestingly, but to a lesser extent, both higher and lower abundances of different *Bifidobacterium* ASVs (Fig. 3). These PCo-bacteria correlations were confirmed using metagenomic sequencing (Supplementary Fig. 4), though simultaneously providing better species resolution. Notably, PCo2 indicated higher abundances of *K. oxytoca*, indicating a species-specification to the unidentified *Enterobacteriaceae* ASV from 16S-based sequencing. From 16S data, we calculated the Shannon index and number of observed species as two complementary measures of alpha diversity. The PCo-s were orthogonal and showed very weak rank correlations with one another, suggesting that each of them captures an independent aspect of the variance in gut bacterial community composition (Supplementary Fig. 5). The two alpha diversity indices were, as expected, moderately correlated with one another; furthermore, observed species had a moderate negative correlation with PCo1 (Supplementary Fig. 5).

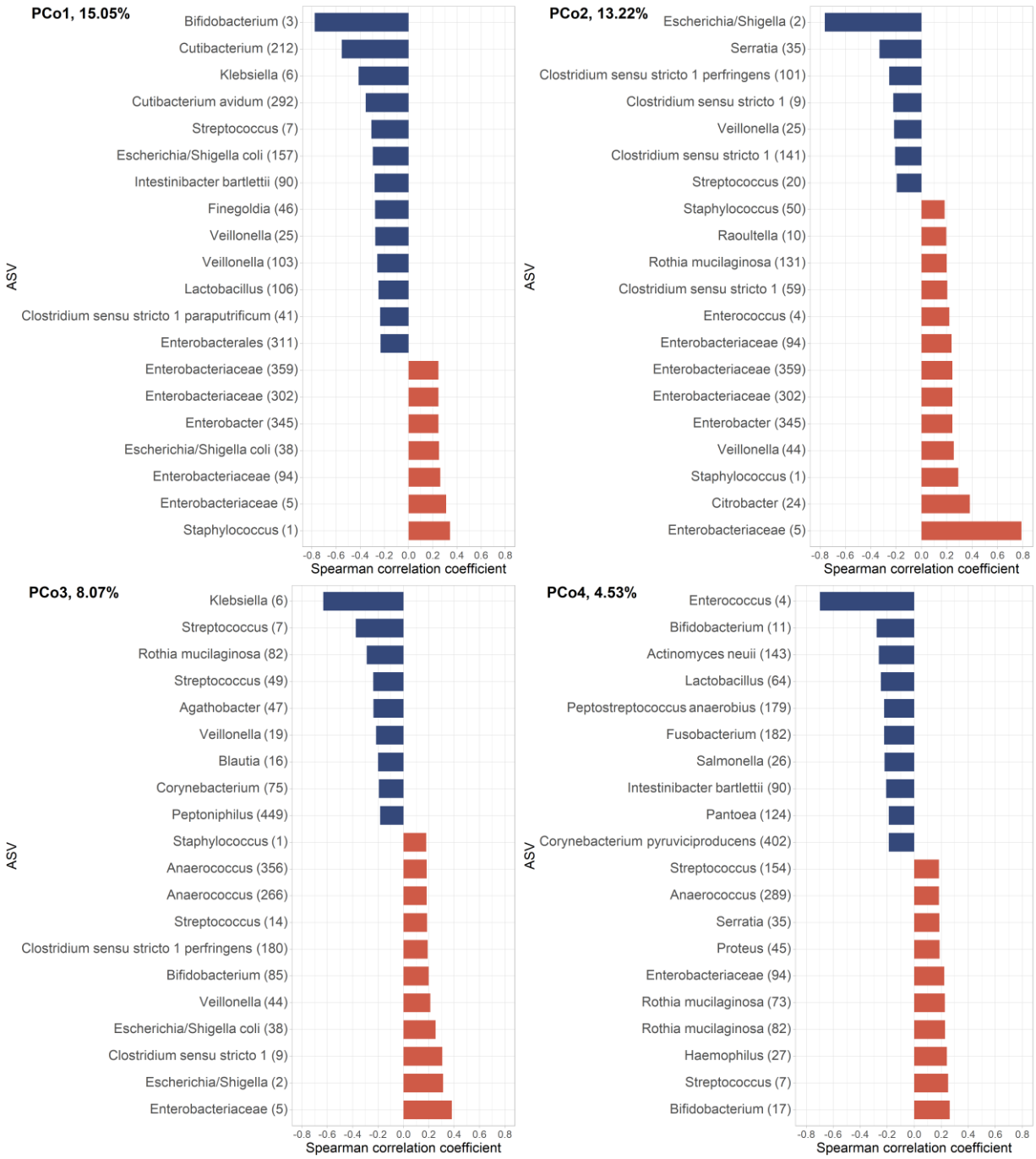

Fig. 3 Dimensionality reduction of the microbiota community composition data. Bacterial ASV correlations with the first four orthogonal principal coordinates (PCo), showing the top 20 strongest correlations for each PCo. The % refers to the variance explained by each of the PCos. Red indicates positive and blue negative correlations between the PCo-s and ASVs.

The four beta-diversity PCo-s and two alpha diversity indices were then used as main predictors of interest in studying the relationships between gut microbiota and MRI biomarkers of EoP. We focussed on whole-brain imaging metrics capturing brain size (tissue volumes), microstructure derived from diffusion tensor imaging (DTI; fractional anisotropy [FA], radial diffusivity [RD]) and neurite orientation dispersion and density imaging (NODDI; neurite density index [NDI], orientation dispersion index [ODI], isotropic volume fraction [ISO]), and cortical morphometry (gyrification index, thickness, sulcal depth, curvature, surface area). For contextualisation of the image features in respect to GA at birth and at scan, please see Supplementary Table 7.

PCo1 negatively correlated with total brain tissue and absolute white matter volume, and positively with relative dGM volume (Fig. 4a). The incremental R^2 upon adding the PCo1 to a null model was 2.6% for total brain tissue, 5.4% for white matter, and 8.3% for dGM relative volume (Supplementary Table 8). There was also a nominally significant association between relative cortical volume and PCo2 (incremental R^2 = 2.6%). However, no volumetric association remained significant after multiple comparison adjustment.

In contrast, there were significant associations between the microbiota and dMRI features of EoP after correction for multiple tests (Fig. 4b, Supplementary Table 8). PCo2 associated with dGM microstructure (incremental R^2 was 6.4% for ODI and 2.3% for NDI) and ODI in the cortex (incremental R^2 7.8%); PCo3 associated with measures of global white matter microstructure (gRD, gNDI and gISO; incremental R^2 was 5.6%, 2.7% and 6.0%, respectively); and PCo4 associated with cortical complexity (thickness; incremental R^2 5.2%) and microstructure (ODI; incremental R^2 = 7.5%). Microbiota richness (number of observed species) also associated with dGM microstructure (incremental R^2 was 3.9%, 3.4%, 4.3% and 2.7%, for FA, NDI, ODI and RD, respectively) as well as ODI in the white matter (incremental R^2 = 4.3%).

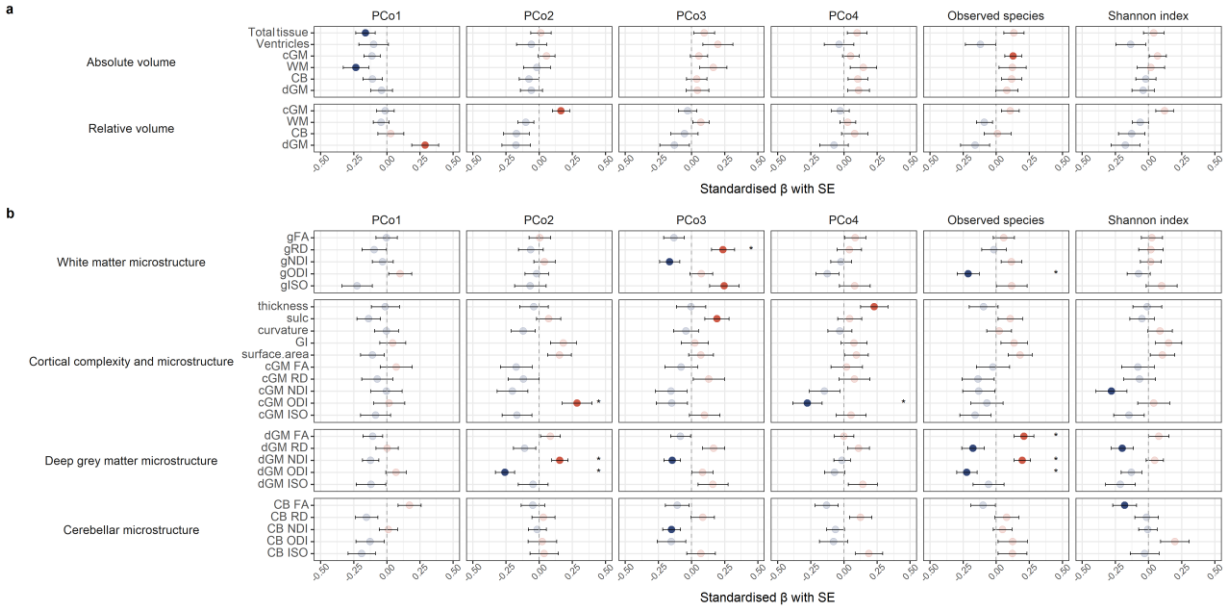

Fig. 4 Microbiota associations with brain volumetric (**a**) and microstructural (**b**) measures. Models are adjusted for gestational age at birth and at scan; microbiota PCo-s and alpha diversity metrics were adjusted for gestational age at sampling via linear regression, retaining the residuals. Full colour points indicate nominal p-value < 0.05; asterisks (*) indicate Benjamini-Hochberg (BH)-method-adjusted p-value < 0.25. Red indicates positive and blue negative associations. Relative volumes are calculated by normalising to total tissue volume (the sum of the volumes of cortical grey matter, white matter, deep grey matter, cerebellum, brainstem, hippocampi and amygdalae). FA = fractional anisotropy; RD = radial diffusivity; NDI = neurite density index; ODI = orientation dispersion index; ISO = isotropic volume fraction; cGM = cortical grey matter; dGM = deep grey matter, CB = cerebellum; sulc = sulcal depth; GI = gyrification index, g = general factor. Sample sizes (total n=79): volumetric and cortical structural complexity analysis = 76, white matter microstructure analysis = 74, and cortical and deep grey matter and cerebellar microstructural diffusion analysis = 74.

The statistically significant microbiota-brain associations after FDR correction (except for the correlation between observed species and gODI), remained significant in sensitivity analyses where we adjusted for birthweight z-score and sex, and excluded infants with NEC (Supplementary Table 9).

PCo-s capture complex patterns of variation within bacterial communities; therefore, to better understand how specific bacterial biomarkers may be related to brain features, we performed post-hoc analysis using MaAsLin2 for those MRI features that showed significant associations with gut

microbiota in PCo- and alpha diversity-based analyses. These results were partially in line with those obtained using the microbial community PCo-s (Fig. 5; Supplementary Table 10). *Bifidobacterium*, the strongest driver of the PCo1, was not significantly associated with any of the brain microstructural measures tested. In line with the PCo2-dGM microstructure findings, *Escherichia/Shigella*, the strongest negative driver of PCo2, showed significant associations with FA (q = 0.204), NDI (q = 0.004), and ODI (q = 0.061) in dGM. Also in line, *Enterobacteriaceae*, the strongest positive driver of PCo2, correlated significantly with dGM ODI (q = 0.025). *Klebsiella*, the strongest negative driver of PCo3, was ranked at the top of the list of associations with gRD (q = 0.328), and was interestingly significantly associated with NDI (q = 0.089) and ODI (q = 0.162) in dGM. In contrast, *Enterococcus*, the strongest negative driver of PCo4, was not significantly associated with any of the MRI markers.

These analyses revealed further relationships between brain MRI features and bacterial taxa beyond the main drivers of the community composition variance. Notably, different *Veillonella* ASVs positively correlated with dGM FA/NDI (q range 0.018 – 0.209) and negatively with ODI (q range 0.083 – 0.115).

Analyses using the shotgun data showed similar bacteria-brain associations (Supplementary Table 11). Importantly, these replicated the *E.coli*, *Klebsiella* spp. (*oxytoca, michiganesis, pneumoniae*) and *Veillonella parvula* correlations with dGM microstructure, and *E. coli* correlations with cortical ODI. Interestingly, using these data, *Bifidobacterium breve* positively correlated with FA in the dGM.

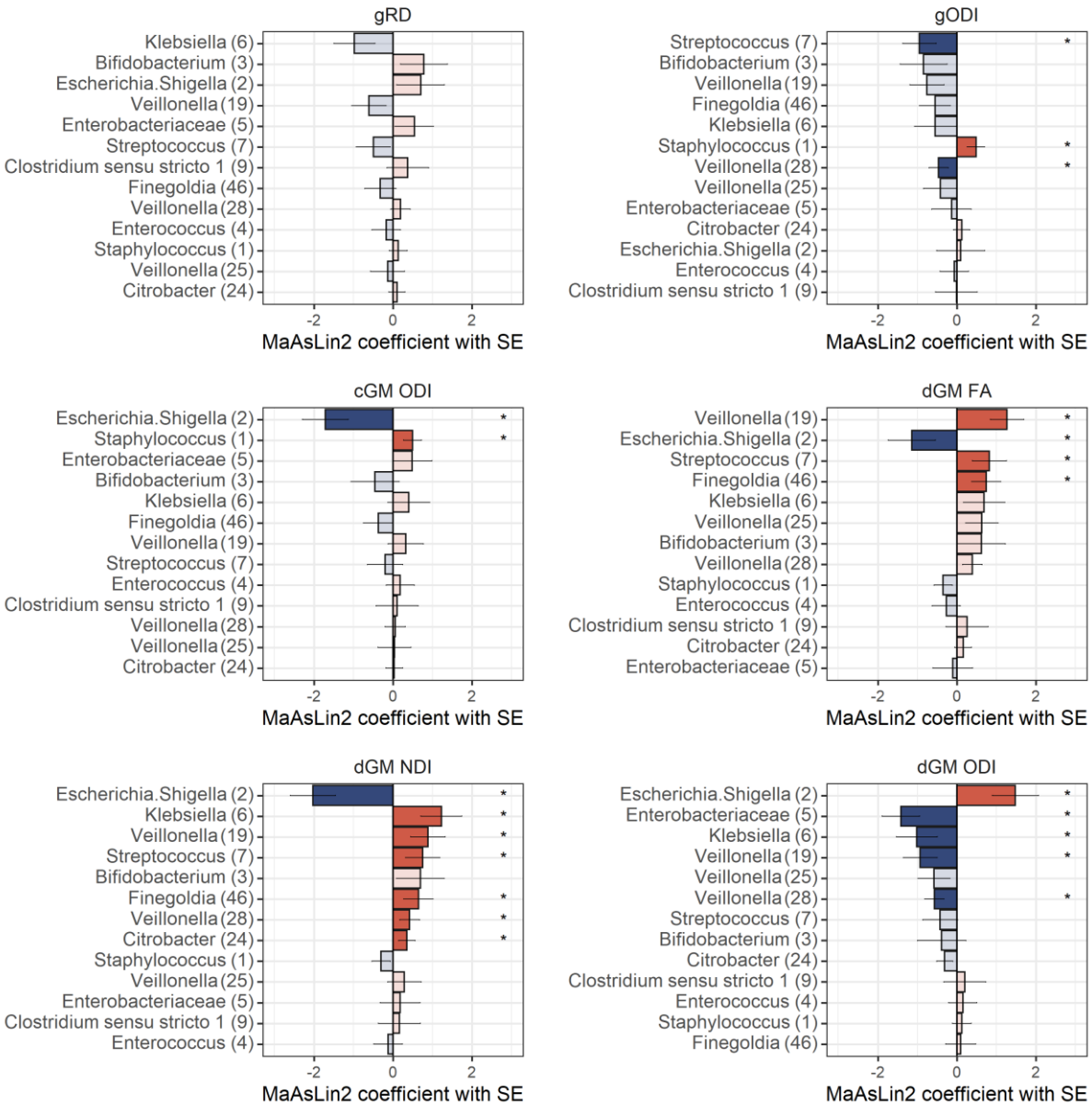

Fig. 5 Taxa-level analyses correlating brain microstructural features with the relative abundances of ASVs. Analyses were conducted using MaAsLin2, testing differences in ASVs present with at least 1% of abundance in at least 10% of samples (n=13 ASVs). ASVs are ordered by the strength of association with each brain imaging feature. Lengths of the bars correspond with the MaAsLin2-model coefficient, which relates to the strength of the association. Error bars indicate the standard error (SE) of the model coefficient. Full colour bars and asterisks (*) indicate Benjamini-Hochberg (BH)-method-adjusted p-value < 0.25. Red indicates positive and blue negative associations. ASV = amplicon sequence variant; MaAsLin = Microbiome Multivariate Association with Linear Models; FA = fractional anisotropy; RD = radial diffusivity; NDI = neurite density index; ODI = orientation dispersion index; cGM = cortical grey matter; dGM = deep grey matter, g = general factor.

Bacterial functional capacity and brain microstructure

To probe the functional implications of the bacteria-brain relationships, we calculated gut-brain modules[36] (GBMs). Among the most abundant GBMs were several related to excitotoxic pathways including glutamate and quinolinic acid metabolism (Fig. 6).

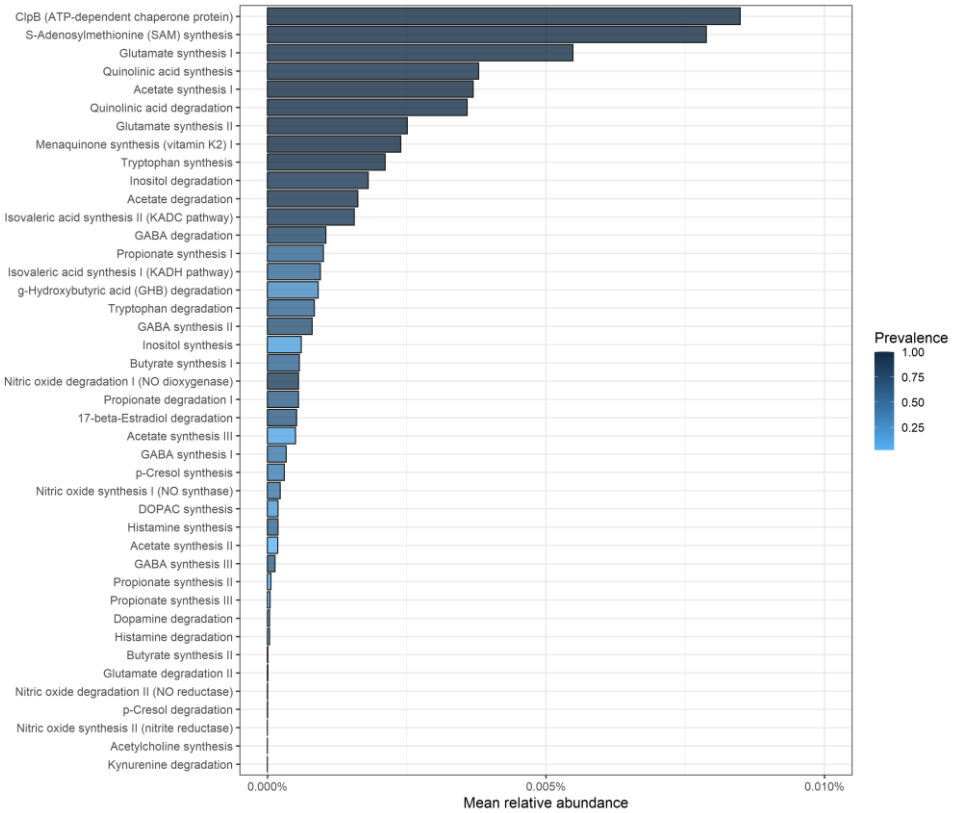

Fig. 6 Mean relative abundance of the gut-brain modules reflecting functional potential of the metagenome; bars are coloured by the prevalence of the modules. 42 out of 56 GBMs were detected in the microbiome-MRI matching dataset; all are present in at least two samples.

PCo1 correlated the strongest with modules related to quinolinic acid and menaquinone synthesis; PCo2 correlated with modules related to degradation of tryptophan, and inositol; PCo3 correlated with modules for the synthesis of S-adenosylmethionine (SAM) and degradation of tryptophan; and PCo4 correlated with GABA and inositol degradation (Fig. 7). For additional functional interpretation of the PCo-s with regard to GMMs, see Supplementary Fig. 6.

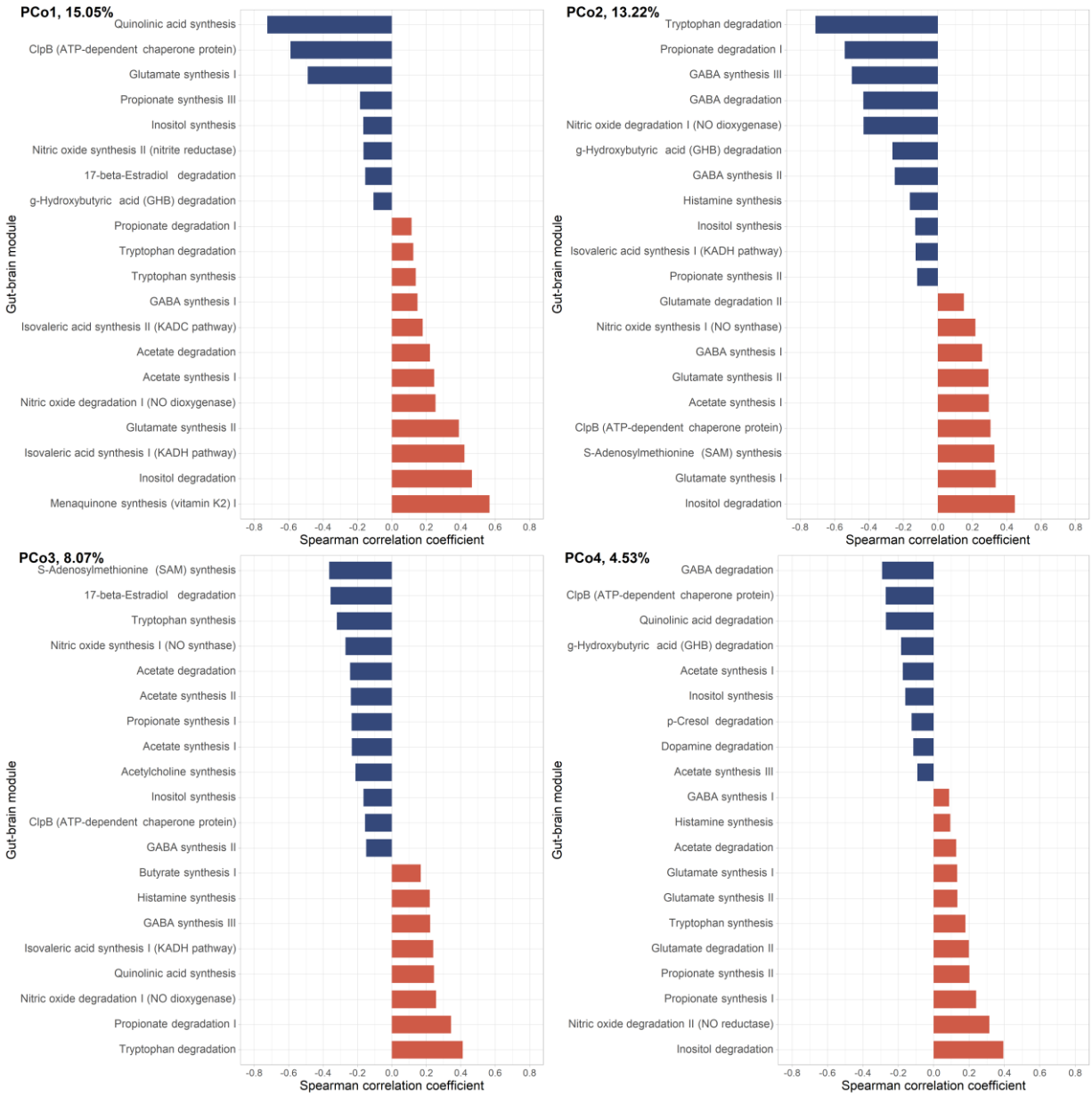

Fig. 7 Gut-brain module correlations with the first four orthogonal principal coordinates (PCo) calculated from 16S rRNA beta diversity data, showing the top 20 strongest correlations for each PCo. The % refers to the variance explained by each of the PCo. Red indicates positive and blue negative correlations between the PCo-s and gut-brain modules.

We then studied the relationships between GBM abundances and those MRI markers that were identified as significantly associated with the gut microbiota PCo-s or alpha diversity using MaAsLin2. This revealed the strongest associations between modules related to the capacity of propionate and tryptophan metabolism and NODDI measures in the deep and cortical grey matter (Fig. 8, Supplementary Table 12). dGM microstructure additionally associated with modules related to caseinolytic peptidase B (ClpB), SAM and glutamate synthesis – three most abundant GBMs identified.

Lastly, when investigating which bacteria contribute to the brain-associated GBMs, in line with PCo-GBM correlations (Fig. 7), we found that *E. coli* is the strongest contributor to the modules related to the capacity of tryptophan and propionate degradation, and *Klebsiella* spp. have high contributions to the capacity of propionate synthesis (Supplementary Fig. 7). *Bifidobacterium* spp. were among the main contributors to the most abundant GBMs.

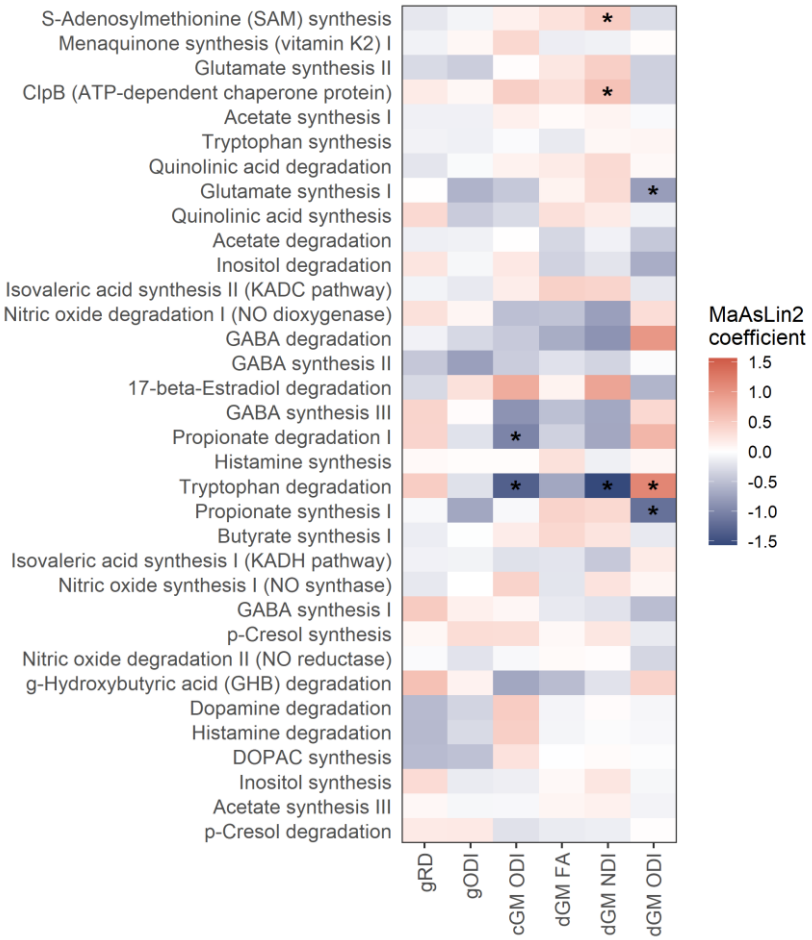

Fig. 8 Gut-brain modules in correlation with brain microstructural features. Analyses were conducted using MaAsLin2, testing differences in gut-brain modules present in at least 10% of samples (n=34 modules). Modules are ordered by the prevalence in the dataset. Colour corresponds to MaAsLin2-model coefficient, which relates to the strength of the association, with blue indicating negative and red positive correlations. Asterisks (*) indicate Benjamini-Hochberg (BH)-method-adjusted p-value < 0.25. FA = fractional anisotropy; RD = radial diffusivity; NDI = neurite density index; ODI = orientation dispersion index; cGM = cortical grey matter; dGM = deep grey matter, g = general factor.

Discussion

We characterised the gut microbiome of preterm infants using 16S rRNA gene and shotgun metagenomic sequencing, and determined the most influential clinical drivers of the preterm microbiota during NICU care. For the first time, we integrated metagenome data with multimodal brain MRI to uncover associations between microbiota community composition, diversity and functional capacity, and the EoP.

Neonatal microbiota development

There was a substantial shift in microbiota diversity and community composition between preterm birth and hospital discharge. Shortly after birth, the microbiota of the majority of infants was dominated by the facultative anaerobe *Staphylococcus*. By the time of NICU discharge, the microbiota diversity had increased and most preterm infants had gut microbiota profiles with high relative abundances of either *Bifidobacterium* or *Enterobacteriaceae*, mainly *Klebsiella* spp. However, some infants retained community compositions high in *Escherichia/Shigella* or *Enterococcus.* These observations are consistent with previous reports of a dynamic development of the gut microbiota over the neonatal period in preterm infants, which includes increase in bacterial alpha diversity and a shift in community composition[33,37].

Differences in the meconium microbiota of term and preterm infants

There were small differences in bacterial community composition between term and preterm meconium with higher abundance of *Escherichia/Shigella* and *Streptococcus* in the preterm group – a profile that has been reported previously[38]. Preterm infant meconium had higher microbiota richness, which might reflect the slightly higher postnatal age at sampling in the preterm group due to delayed passage of meconium in preterm infants, and is consistent with a decrease in alpha diversity in the first days of life due to environmental filtering before a gradual increase coinciding with actual colonisation[33,39]. An important technical consideration for interpreting meconium microbiota data is that only a small proportion of term infant meconium samples yielded sufficient amount of DNA for sequencing, which limits power to detect differences. Yet, meconium has low bacterial DNA[40,41], with relatively higher detection in preterm infants[40], suggesting that meconium of healthy term-born infants contains very low bacterial biomass. Even among the preterm group, only a minority of meconium samples had sufficient DNA yield for shotgun sequencing. Thus, the profiles may not be representative of the majority of meconium samples; this could explain some of the differences observed in the results with 16S-based vs shotgun sequencing.

Drivers of the preterm gut microbiota at birth and at NICU discharge

Low birth GA did not correlate with bacterial community composition at TP1, but it was the strongest covariate at TP2, which suggests there is an allostatic load of prematurity-related co-exposures that shape the preterm microbiota. Low GA associated positively with the abundance of *Veillonella* – a signature taxa in the 4-month-old term infant microbiota, associated with reduced oxygen concentration and utilisation of lactic acid[42]. Given that low GA also associated negatively with the abundance of *Staphylococcus*, these findings suggest a “younger-looking” microbiota at the time of NICU discharge in infants born at a higher GA.

Delivery mode had the strongest correlation with the bacterial community composition in meconium, manifesting predominantly as higher abundances of *Staphylococcus* in C-section-born infants. This has previously been reported in term infants[43] but there is more variability in the preterm literature about the impact of mode of delivery[22]; these data provide additional information from a new cohort. At TP2, delivery mode was not associated with microbiota composition, which could reflect either “recovery” of gut microbiota profiles following C-section birth[43], or an overshadowing by prematurity-related co-exposures. In addition to low birth GA, infant sex and antibiotic exposure contributed to microbiota composition at TP2. Recent studies have investigated the role of sex on gut microbiota[44], however, only a few have done so in infancy, with mixed results[33,45,46]. With both 16S-based and shotgun sequencing we found the strongest evidence for higher abundance of *Streptococcus* in male babies. Sex differences in this context are interesting because preterm boys have a higher risk of major morbidities than preterm girls[34]. In line with previous studies[47], we report higher abundance of *Klebsiella* in infants exposed to antibiotics during their NICU stay. Furthermore, similarly supporting previous findings[47], exposure to antibiotics rather than length of exposure associated with microbiota composition in preterm infants, suggesting an exquisite sensitivity of the preterm microbiota to antimicrobial treatment.

Microbiota-brain interactions: relevance to encephalopathy of prematurity

We took two complementary approaches to study correlations between the microbiome and brain structure: we applied dimensionality reduction[48] to construct latent variables capturing the main variance of bacterial composition, followed by post-hoc MaAsLin2 analyses.

Results from both methods suggested the strongest correlations between the relative abundances of *Escherichia/Shigella* (*E. coli* from shotgun sequencing) and dGM and cortical microstructure, particularly measures derived from NODDI, and between *Enterobacteriaceae* (*Klebsiella* spp. using

shotgun sequencing) and dGM microstructure. This suggests that gut microbiota associates with cellular and dendritic morphology as previously demonstrated in rodent models of microbiota disruptions[49]. Morphological changes in dGM nuclei are commonly observed in preterm infants[50–52]; these associate with reduced microstructural integrity in the white matter and poorer neurodevelopmental outcomes[5]. In addition, preterm birth associates with alterations in cortical microstructure and morphology at TEA[53]. *Escherichia/Shigella* and *Klebsiella* have been linked with neurodevelopment previously, primarily with better and worse outcomes, respectively[24,26,28,54]. Thus, the current bacteria-brain findings are intriguing, given the age- and birth GA-associations for the NODDI parameters (Supplementary Table 7). For example, dGM NDI is positively and ODI negatively associated with GA at scan, suggesting that decreased abundance of *Escherichia* and increased abundance of *Klebsiella* spp. associate with microstructural markers related to more mature dGM microstructure. However, the functional/behavioural implications of microstructural changes in the neonatal grey matter are not yet established, leaving uncertainty in the assignment of positive/negative valence to the bacteria-brain relationships. Nevertheless, these findings contribute to the literature highlighting the importance of these taxa in the microstructural development of deep and cortical grey matter in preterm infants.

Post-hoc analyses also revealed bacteria-brain relationships that were not captured as the main drivers of the first four beta diversity PCo-s. Specifically, *Veillonella parvula*, which associated with degree of prematurity, correlated with dGM microstructural parameters, following the same direction of effect as GA at scan (Supplementary Table 7). *Veillonella* has been associated with neurobehavioural outcomes, including motor and temperament development[13]. *Veillonella* could play different roles in brain function and behaviour at different developmental phases, and it remains to be established to what extent these relationships may be mediated by brain microstructure around the time of birth.

Calculation of GBMs allowed functional interpretation of the bacteria-brain relationships. In particular, the PCo indicated by the abundances of *Escherichia* and *Enterobacteriaceae/Klebsiella oxytoca*, correlated the strongest with the capacity for tryptophan degradation. Indeed, MaAsLin2 analyses showed that this module's abundance correlated with the microstructure in dGM and cortex. *E. coli* was the most substantial contributor to this functional property of the microbiome. Tryptophan metabolism has been suggested as one of the key gut-brain communication mechanisms in preclinical and human observational studies[10]. *E. coli* degrades tryptophan into indole, which regulates gut epithelial cell function and immune response[55], as well as central nervous system inflammation via astrocytes[56]. Thus, our results suggest that *E. coli* may interact with brain microstructural development via tryptophan metabolism.

Synthesis and degradation of the short-chain fatty acid (SCFA) propionate correlated with ODI in dGM and cortex, respectively. The strongest contributors to these modules were *Klebsiella* spp. and *E. coli*, respectively. Propionate, acetate and butyrate are among the most abundant SCFAs in the human body. SCFAs have wide-ranging functions[57], including (neuro)immune modulation, and propionate has been demonstrated to impact the blood-brain-barrier[58]. Future studies, including metabolomics, are required to validate the current findings, and to identify to what extent bacterial-derived propionate directly interacts with the brain.

Bifidobacterium is the predominant bacterium in vaginally delivered breastfed infants during the first year of life, and several studies have identified positive correlations between *Bifidobacterium* abundance and neurobehavioural outcomes[13], including in preterm infants[25]. It is sometimes used as a probiotic to prevent NEC in preterm infants, though clinical efficacy is uncertain and we are not aware of studies of its impact, if any, on neurodevelopment[59]. We found some suggestive evidence that the primarily *Bifidobacterium*-driven PCo1 correlates with total brain and white matter volume

and with relative dGM volume, reflecting improved brain growth in association with higher abundance of *Bifidobacterium*. We also found that *Bifidobacterium* spp. were one of the main contributors to the three most abundant GBMs in this preterm dataset, which significantly correlated with dGM microstructure: ClpB, SAM and glutamate synthesis. This may suggest that *Bifidobacterium* involvement in metabolic pathways may be important for brain structural development. However, these potential relationships between *Bifidobacterium* and brain structure need to be replicated in an independent cohort. A recent Cochrane review[59] concluded that further large, high-quality trials are needed to inform clinical practice about probiotic use for the prevention of NEC in preterm infants. Our data indicate that assessment of neurodevelopment should be incorporated into future studies of safety and efficacy of probiotics in preterm infants.

Strengths and limitations

The main strength and uniqueness of this study is the linked microbiome-MRI dataset. There is a scarcity of metagenomics data alongside multi-modal neuroimaging, particularly in the neonatal population, making this a valuable contribution to the microbiota-neuroimaging field. We evaluated infants born at <32 weeks' gestation, who are at an especially high risk of adverse neurocognitive outcomes. The clinical profile of the cohort, the absence of major parenchymal lesions, and the similarities of microbiota community composition with other studies, suggest that it is representative of the majority of survivors of neonatal intensive care.

Low biomass samples, such as those collected from neonates, are at an increased risk for biases due to possible bacterial DNA contamination from processing reagents and environment[60]. We included control samples, which enabled to investigate the environmental background and remove contaminant taxa from the dataset. Furthermore, the inclusion of shotgun metagenomic sequencing alongside 16S enabled us to investigate within-study replicability and probe functional capacity.

The study has some limitations. Whilst the sample size was larger than that of previous work integrating microbiota with neuroimaging in infancy and childhood[28,48,61–65], it is still a limitation given the high inter-individual variation both in brain microstructural as well as in the microbiota development in preterm infants. Small samples and high heterogeneity coupled with the multidimensional nature of both microbiota sequencing and neuroimaging datasets and high analytic freedom are the main limitations of microbiota-neuroimaging studies, leading to reduced power and variability in the results. To reduce dimensionality, we focussed on whole-brain measures capturing EoP. However, this may have hindered the detection of more specific brain regions associated with microbiota; future studies with larger sample sizes are needed to investigate the regional-specificity of the observed global effects. PCo analysis and calculation of GBMs from the microbiome data allowed for a principled way of data reduction. There is rapid development of the gut microbiota in the neonatal period, thus, wide age range of sampling could have introduced noise in the microbiota-brain relationships; to mitigate this, we adjusted for age at microbiota sampling at NICU discharge. The sample was not sufficiently powered for age- or sex-stratified analyses.

Finally, the microbiota-brain association analysis was cross-sectional with the timepoints chosen to capture EoP and the allostatic load of prematurity on the gut microbiome. However, this limits causal inference: the relationships observed could reflect a separate process causally linked to the development of gut microbiota and brain structure. Nevertheless, preclinical data shows that colonisation of germ-free mice with preterm microbial communities associates with poor growth, systemic and neuroinflammation, delayed neuronal development and myelination, disrupted brain microstructural connectivity, and behavioural deficits[66,67], supporting a causal relationship.

In conclusion, the results contribute to understanding microbiota-brain interactions following preterm birth and suggest that microbiota modification is a potential new avenue for neuroprotection during neonatal intensive care.

Methods

Participants

Participants were preterm infants (GA at birth <33 weeks) and term-born controls recruited as part of a longitudinal cohort study designed to investigate the effects of preterm birth on brain structure and long-term outcome[29]. Recruitment, sampling and MRI acquisition were at the Royal Infirmary of Edinburgh, UK, between 2016-2021. The study was conducted according to the principles of the Declaration of Helsinki, and ethical approval was obtained from the UK National Research Ethics Service (South East Scotland Research Ethic Committee 16/SS/0154). Parents provided written informed consent.

Exclusion criteria were death during neonatal period, major congenital malformations, chromosomal abnormalities, congenital infection; infants with overt parenchymal lesions (cystic periventricular leukomalacia, haemorrhagic parenchymal infarction), post-haemorrhagic ventricular dilatation, or contra-indications to MRI were excluded from MRI analyses. Term-born infants who required admission to the NICU were also excluded.

All infants were cared for in the Neonatal unit of the Simpson Centre for Reproductive Health, Royal Infirmary of Edinburgh, with standardised feeding, antibacterial and antifungal guidelines. Preterm infants admitted to the NICU in the Simpson Centre for Reproductive Health are not routinely administered any pro- or prebiotic supplements. Clinical data was collected from antenatal and neonatal electronic patient records; see Supplementary materials for details of clinical data definitions.

Gut microbiota

Faecal sample collection and processing

Faecal material was collected from dirty diapers by parents, NICU staff or research team. The samples were frozen at -20°C directly after sample collection prior to transfer to a -80°C freezer in the Queens Medical Research Institute (QMRI, University of Edinburgh) until further analyses; no preservation buffers were used. Faecal material was collected from the first bowel movement (meconium; TP1) from term and preterm infants, and a second faecal sample was collected from preterm infants prior to discharge from the NICU (pre-discharge sample; TP2), which was around TEA. When preterm infants were transferred to another NICU prior discharge, the second sample was collected prior to transfer. A total of 143 meconium and 107 pre-discharge samples were collected during the study period; 44 preterm infants had both samples obtained.

DNA isolation

The bacterial DNA from faecal samples was extracted at the QMRI as previously described[68] involving phenol/bead beating in combination with the Agowa Mag Mini DNA Isolation Kit (LGC genomics, Germany). See details in Supplementary materials.

To avoid potential cross-contamination from high-abundant to low-abundant samples, DNA from meconium and pre-discharge faecal samples was isolated on separate days. Each extraction was accompanied by negative (200 µl of lysis buffer) and positive controls (ZymoBIOMICS Microbial Community Standard [Zymo Research, USA] and/or a convenience saliva sample).

The amount of extracted bacterial DNA was determined by quantitative polymerase chain reaction (qPCR) as previously[68,69] with universal primers and probes targeting the 16S-rRNA gene (forward: 5′-CGAAAGCGTGGGGAGCAAA-3′, reverse: 5′-GTTCGTACTCCCCAGGCGG-3′, TAMRA probe: 6FAM-ATTAGATACCCTGGTAGTCCA-MGB; Life Technologies, USA).

16S rRNA gene sequencing

Samples that yielded DNA concentration of >0.18 pg/µl were considered for 16S rRNA gene sequencing (Supplementary Fig. 1).

V4 hypervariable region of the 16S rRNA gene was amplified as previously[70]: amplicon libraries were generated by PCR using barcoded primers (515F (5'-GTGCCAGCAGCCGCGGTAA-3') and 806R (5'-GGACTACCAGG-GTATCTAAT-3'[71]), using 5µl of DNA as template. Two mock DNA communities (see Supplementary methods) and a non-template control were included in each MiSeq PCR plate and amplified alongside the samples and isolation positive and negative controls.

The amplified DNA concentration was quantified using Quant-iT™ PicoGreen® dsDNA Assay Kit (Life Technologies, USA) and visualised on gel electrophoresis to ensure successful amplification. The amplicons were pooled at equimolar amounts and purified using a combination of agarose gel purification (GeneJET Gel Extraction and DNA Cleanup Micro Kit) and purification by AMPure XP magnetic beads (Thermo Fisher Scientific, MA, USA).

As previously[70], 16S rRNA gene sequencing was performed using the MiSeq Reagent Kit v2 on the Illumina MiSeq platform (Illumina, Eindhoven, the Netherlands). Sequencing was performed by Edinburgh Genomics (University of Edinburgh, UK) on a total of 191 samples, 23 negative and 18 positive controls in one run.

Bioinformatic processing and quality control of 16S rRNA sequences

16S rRNA gene sequencing data processing was performed in R (version 4.2.1)[72] as previously described[73]. Paired-end raw reads were filtered and trimmed (maxEE = 2; truncLen = 200/150 bp for forward and reverse reads, respectively), merged, denoised, chimera filtered and binned into ASVs using the DADA2 (version 1.16.0) in R[74]. Taxonomy was assigned using the DADA2 implementation of the naïve Bayesian classifier using the Silva v138.2 reference database. Species-level annotations were added using the *addSpecies()* function. ASVs not assigned to the kingdom Bacteria or assigned to the family Mitochondria or class Chloroplast were removed.

Contamination was assessed using *decontam* package in R[75] ("combined" method, default parameters), combined with manual inspection of putative contaminating ASVs (see details in Supplementary methods). We filtered out ultra-rare taxa by only including ASVs with a relative abundance >0.1% in at least two samples in the final dataset[76]; samples that had a read count of less than 5000 following decontamination steps were excluded. Following data quality control, the 16S-based sequencing produced a mean of 35416 reads (range 7534 – 109456) per sample. The ASV table contained 174 ASVs.

In the final analytic sample, all participants with TP2 samples and 70/136 (51.5%) TP1 samples were included (Supplementary Fig. 1). Included participants with TP1 samples were more likely obtained from preterm participants (Supplementary Table 13).

Metagenomic shotgun sequencing and bioinformatic processing

Samples with 16S qPCR concentration >0.8ng/µl (n=121) alongside three saliva positive controls and eight isolation negative controls were considered for shotgun metagenomic sequencing at Novogene facility (Novogene Co., Ltd, Cambridge, UK). Sequencing was performed on the NovaSeq 6000 platform (Illumina) with a read length of 150-bp paired-end reads producing 9G raw data per

sample. Shotgun sequencing failed for all negative controls, indicating absence or very low abundance of biological material, and one biological sample from TP1.

Data pre-processing and annotation was performed by Edinburgh Genomics. Whole metagenome shotgun sequencing produced a mean of 37410649 (range 2512236 – 81101422) raw reads per sample. The raw reads were cleaned using cutadapt (v3.5)[77]. Adapters were removed, reads were cut when the quality dropped below 30, and reads shorter than 50 bases were removed. Reads belonging to the host were removed by bowtie2 (v2.4.1)[78] using Homo Sapiens (GRCh38) as a reference. Files sequenced on multiple lanes but belonging to the same sample were merged into single forward and reverse files.

Taxonomic profiling was performed using MetaPhlAn (v3.1)[79] with the standard database (mpa_v31_CHOCOPhlAn_201901). Functional profiling was performed using HUMAnN (v3)[79] with the default chocophlan (chocophlan.v201901_v31) and the uniref90 databases (uniref90_annotated_v201901b). As MetaPhlAn and HUMAnN do not use paired information of reads, all reads of a sample were merged into a single file and used for taxonomical/functional assignment. As shotgun metagenomic sequencing was performed on higher density samples, the relative contribution of potentially contaminant taxa is smaller, thus, no further quality controls/decontamination on species/functional level were performed. Functional gene families data was grouped to KOs using the *humann_regroup_table* function, both for community-level totals and species-stratified gene families. The KO abundance data table was total-sum-scaled (TSS) to relative abundances using the *humann_renorm_table* function; the unmapped and ungrouped reads were taken into account for TSS-normalisation, but excluded from downstream statistical analyses. From the normalised KO table we computed GMMs[30] and GBMs[36] using the omixer-rpmR library[31] using the default settings for both community and taxon-stratified levels. Shotgun sequencing dataset contained a total of 223 species, 94 GMMs, and 43 GBMs.

Magnetic resonance imaging

Imaging data acquisition

Infants were scanned at TEA at the Edinburgh Imaging Facility, Royal Infirmary of Edinburgh, University of Edinburgh, UK, using a Siemens MAGNETOM Prisma 3T MRI clinical scanner (Siemens Healthcare, Erlangen, Germany) and a 16-channel phased-array paediatric head coil in natural sleep as previously described[80]. Each acquisition was inspected contemporaneously for motion artefact and repeated if there had been movement but the baby was still sleeping; diffusion MRI acquisitions were repeated if signal loss was seen in three or more volumes.

MRI acquisition protocols are detailed in the study protocol paper[29]. This study included: a 3D T2-weighted (T2w) structural scan, and a multishell axial diffusion MRI (dMRI) scan. See details in Supplementary methods.

Structural images were reported by a paediatric radiologist with experience in neonatal MRI (AJQ). Images with evidence of post-haemorrhagic ventricular dilatation, cystic periventricular leukomalacia or central nervous system malformation were excluded from subsequent analysis.

Imaging data pre-processing

Details on dMRI processing have been previously published[80]; see Supplementary methods for details. The structural images were processed using the minimal processing pipeline of the developing Human Connectome Project (dHCP)[81] to obtain the bias field corrected T2w, brain mask, tissue segmentation and the different tissue probability maps. The mean b0 EPI volume of each subject's dMRI acquisition was co-registered to their structural T2w volume using boundary-based registration using FMRIB's Linear Image Registration Tool (FLIRT)[82].

From the diffusion images we calculated the DTI (FA, RD) and NODDI (NDI, ODI and ISO) maps. The DTI model was fitted in each voxel using only the b = 750 s/mm^2 shell. NODDI maps were calculated using all shells and the recommended values of the parallel intrinsic diffusivity for neonatal brain tissues[83,84] using the original NODDI MATLAB toolbox (http://mig.cs.ucl.ac.uk/index.php?n=Tutorial.NODDImatlab).

Selection of image features

Volumes. We calculated the volumes of the total tissue, cortical grey matter, deep grey matter, white matter, cerebellum, and the ventricles from the tissue parcellation obtained from the dHCP pipeline[81]. For cortical grey matter, deep grey matter, white matter and the cerebellum both raw and relative (i.e. normalised to total tissue volume) volumes were obtained to quantify absolute growth of the tissues as well as that relative to total brain growth, respectively.

Grey matter microstructure. For cortical and deep grey matter and the cerebellum, the mean DTI and NODDI metrics were calculated, using the recommended value for the parallel intrinsic diffusivity for neonatal grey matter (1.25 μm^2/m) for NODDI map calculations[83]. For the cortex, mean gyrification index, thickness, sulcal depth, curvature and surface area as measures of cortical complexity/morphometry were also calculated[81].

White matter microstructure. To capture global white matter dysmaturation, we segmented 16 major tracts and derived general factors (g-factors) for each of the DTI and NODDI metrics as described previously[80]. The only difference with the previous work was that the tracts were brought from ENA50 neonatal template space to native space via registration of the FA maps to ENA50 FA template using rigid, affine and symmetric normalization (SyN) implemented in Advanced Normalization Tools[85]. For the tracts, the NODDI metrics were calculated using the recommended values of the parallel intrinsic diffusivity for neonatal white matter (1.45 μm^2/ms)[83].

For contextualisation of the image features, we performed linear regression modelling for each neuroimaging feature as the outcome and GA at birth and at scan as the predictors (Supplementary Table 7). Representative brain maps are provided in Supplementary Fig. 12.

Statistical methods

All statistical analyses were performed in R 4.2.1[72]. Visualisations were plotted using the *ggplot2*[86], *ggpubr*[87] and *cowplot*[88] packages. Where necessary, distribution of variables and regression diagnostic plots were visually inspected to ensure approximate conformation to assumptions; normal distribution was additionally assessed using Shapiro-Wilk's test. P-values from statistical tests were adjusted for multiple comparisons using the Benjamini-Hochberg method[89] separately within each analysis type, producing q-values (see details within each subsection).

Beta diversity and PERMANOVA

Beta diversity was calculated as the Bray-Curtis dissimilarity[90] matrix based on the TSS-normalised (i.e. relative abundances) ASV, species and functional GMMs tables using *vegdist* function (*vegan* package[91]). PERMANOVA, modelled by *adonis2* (*vegan* package[91]) with 1000 permutations, was used to identify differences in overall bacterial community composition. Separate PERMANOVAs were performed for all pairwise comparisons for the different sample types and timepoints; when comparing TP1 vs TP2 composition within preterm infant group we adjusted for repeated measures by constraining the permutations within participant (strata = participant ID). To assess the effects of perinatal covariates, univariable analyses were conducted for each covariate, separately for the timepoints; p-values were adjusted for multiple comparisons across the models. Results with q-value < 0.1 were considered as statistically significant and followed up using differential abundance testing.

For visualisation purposes (Fig. 1a and Supplementary Fig. 2a), we applied hierarchical clustering (*hclust* function) on the ASV- and species-level Bray-Curtis dissimilarity matrices. Calinski-Harabasz and Silhouette width indices were used to determine whether average (ASV data) or complete (species data) linkage was optimal for the different datasets.

Ordination

Principal Coordinates Analysis (PCoA) was performed on the ASV-level Bray-Curtis dissimilarity matrix using the function *pcoa* (*ape* package[92]). Cailliez transformation was applied to correct for negative eigenvalues[93]. The scree plot of the eigenvalues alongside with proportion of variance explained were inspected to determine the optimum number of coordinates to extract. For taxonomic and functional interpretation of the main axes of variance (i.e. the extracted PCo-s), Spearman correlation coefficients were calculated between the PCo scores and the relative abundances of the ASVs, species, GBMs and GMMs.

Alpha diversity

Shannon index and observed species were calculated using the *estimate_richness* function (*phyloseq* package[94]). These indices were calculated based on the ASV table after removal of contaminant taxa but before filtering of the ultra-rare taxa. This full ASV table was rarefied to the minimum sequencing depth (10200 reads before filtering of ultra-rare taxa) using *rarefy_even_depth* function. Linear mixed effects modelling (*lmer* function within package *lmerTest*[95], Satterthwaite's method) was used to assess differences in alpha diversity indices between the sample types and timepoints, fitting participant ID as a random effect to adjust for repeated measures. For observed species, the assumption of normal distribution of model residuals was violated and therefore the values were $\log_{10}$-transformed. Post-hoc analyses were conducted using the package *emmeans*[96]. P-values were adjusted for multiple comparisons for the main effects across the models for the two alpha diversity indices, and separately for the three pairwise comparisons. We then assessed the associations between perinatal covariates and alpha diversity indices in preterm infants at the two timepoints. We calculated Spearman correlation coefficients for the associations between continuous variables and alpha diversity indices; t-tests (TP2) and Wilcoxon rank-sum tests (TP1) were applied to test for the differences in alpha diversity indices between groups of infants based on categorical variables. P-values were adjusted for multiple comparisons separately for the timepoints. Covariates with q-value < 0.1 in univariable models were followed up with multivariable linear regression modelling including all covariates to adjust for the potential confounding effects between the variables.

Associations between gut microbiota and brain MRI features

Baseline linear regression models. First, the microbiota features (PCo-s and alpha diversity indices) were adjusted for GA at sample collection by fitting a linear model of each feature on GA at sample collection and retaining the residuals. We adjusted for sampling age in this manner rather than using it as a covariate in the model with the brain MRI feature as the outcome to avoid spurious correlations between GA at microbiota sampling and brain MRI features. Then, a linear regression model was performed for each residualised microbiota feature as the predictor, each MRI feature as the outcome, and GA at birth and at scan added as covariates. All values were scaled (z-transformed) before fitting the models, resulting in standardised regression coefficients. P-values were adjusted for the FDR across all models separately for volumetric and microstructural/cortical morphometric MRI features. Due to the exploratory nature of the study and given the correlated nature of the neuroimaging measures, results with q-value < 0.25 were considered as noteworthy and investigated further in sensitivity and post-hoc differential abundance analyses. FDR correction of the p-values provides a balance between type I and type II errors; 0.25 is the default threshold in MaAsLin2 and there is precedence of using this cut off in microbiota-brain/behaviour studies[63,97].

To quantify the variance in each brain imaging metric accounted for by the microbiota PCo-s or diversity indices, the incremental R^2 was calculated as the difference between the multiple R^2 of each model with that from the null model including only the covariates (GA at birth and at scan) as predictors. We used analysis of variance (ANOVA) to test whether the baseline model with the microbiota feature as the predictor fit the data significantly better compared to the null model.

Covariate identification and adjustment (sensitivity analyses). The clinical variables that were significantly (q-value < 0.1) associated with microbiota alpha- or beta-diversity at TP2 on ASV-level (sex, birthweight z-score, antibiotics >72h of life, and NEC) were tested for associations with brain MRI features. Two-sample t-tests were used to compare the means of normally distributed continuous features between the groups of the categorical covariates; Wilcoxon rank-sum tests were applied to compare differences in non-normally distributed MRI features; Spearman correlation analysis was used to test for significant associations between birthweight z-score and MRI features. Variables that were nominally significantly ($p < 0.05$) associated with at least one of the brain MRI features were added as covariates in the fully adjusted model. These variables were: birthweight z-score, sex and NEC. Only three infants in the sample were diagnosed with NEC, thus, instead of adding this variable as a covariate, a sensitivity analysis was performed excluding infants with NEC.

Differential abundance testing

MaAsLin2[35] was used to identify bacterial ASV, species and functional capacity biomarkers associated with factors of interest. We applied TSS-normalisation prior to MaAsLin2 modelling. As by default in the method, we considered results with q-values < 0.25 as statistically significant.

In analyses assessing the associations between bacterial abundance and perinatal covariates, models were performed separately for the two timepoints. We tested for the effects on ASVs (16S) and species (shotgun) that were present with at least 1% of abundance (min_abundance = 0.01) in at least 5% of samples (min_prevalence = 0.05); the normalisation method within MaAsLin2 was set to “none”; all other arguments were used as by default. Baseline analyses at TP1 were adjusted for postnatal age at sample. Baseline models at TP2 were adjusted for the degree of prematurity (GA group; very vs extremely preterm) and GA at sample collection. At TP1 we didn’t adjust for GA at birth given the lack of statistically significant association in univariable PERMANOVA; at TP2 we adjusted for GA at sample collection instead of postnatal age given the high collinearity between GA at birth and postnatal age. In fully adjusted models, all clinical variables were tested simultaneously. For species, an additional model was performed for TP1 samples including labour antibiotics in the model.

To identify ASVs, species and GBMs associated with brain imaging features, MaAsLin2 was conducted for those brain MRI features that were significantly (q-value < 0.25) associated with any of the microbiota feature in the baseline models. MaAsLin2 reverses predictors and outcomes compared to PCo-based analyses, thus, to achieve alignment of the MaAsLin2 models with the initial baseline regression model, we first adjusted the brain MRI features for GA at birth and at scan by fitting a linear model of each feature on GA at birth and at MRI, retaining the residuals. These residuals were then used independently as the predictors in the MaAsLin2 models, including GA at faecal sample collection as a covariate. Due to the relatively small sample size in comparison with the number of bacterial taxa, in all analyses, we tested for effects on ASVs and species that were present with at least 1% of abundance in at least 10% of samples; other arguments were as specified above; for GBMs, the default MaAsLin2 parameters were used.

Reporting summary

Further information on research design is available in the Nature Research Reporting Summary linked to this article. We followed the Strengthening The Organization and Reporting of Microbiome

Studies (STORMS) checklist[98] in describing the methodology and reporting results (Supplementary Table 14).

Data availability

Requests for neuroimaging data will be considered under the study's Data Access and Collaboration policy and governance process: https://www.ed.ac.uk/centre-reproductive-health/tebc/about-tebc/for-researchers/data-access-collaboration. 16S and shogun data are available upon request from Theirworld Edinburgh Birth Cohort, University of Edinburgh (james.boardman@ed.ac.uk or https://www.ed.ac.uk/centre-reproductive-health/tebc/about-tebc/for-researchers/data-access-collaboration). The microbiome and metadata are not publicly available due to them containing information that could compromise participant consent.

Code availability

Scripts for the data analysis in this paper are available here: https://git.ecdf.ed.ac.uk/jbrl/neonatal-microbiota-and-brain-dysmaturation.

Acknowledgements

This research was funded in whole, or in part, by the Wellcome [No. 108890/Z/15/Z]. For the purpose of open access, the author has applied a CC BY public copyright licence to any Author Accepted Manuscript version arising from this submission. This work was supported by Theirworld (www.theirworld.org) and was carried out in the Medical Research Council Centre for Reproductive Health, which was funded by Medical Research Council Centre Grant (MRC G1002033). Participants were scanned in the University of Edinburgh Imaging Research MRI Facility at the Royal Infirmary of Edinburgh, which was established with funding from The Wellcome Trust, Dunhill Medical Trust, Edinburgh and Lothians Research Foundation, Theirworld, The Muir Maxwell Trust and other sources. KV was funded by the Wellcome Translational Neuroscience PhD Programme at the University of Edinburgh (108890/Z/15/Z). MJT was funded by the NHS Lothian Research and Development Office. The authors are grateful to the families who consented to take part in the study and to all the University's imaging research staff for providing the infant scanning. We would also like to acknowledge Edinburgh Genomics for executing the 16S rRNA gene sequencing and Heleen de Weerd for the bioinformatic processing of the shotgun data; shotgun metagenomic sequencing was performed at Novogene.

Author contributions

KV, DB and JPB conceived and designed the experiments. GS, DQS and AC recruited the participants. GS, DQS, AC and KV supervised MRI acquisition and collected clinical data. PLP and KV were responsible for the execution and quality control of the laboratory work. MBC and KV performed MRI data quality control and processing. AJQ was responsible for clinical evaluation of MR images. MJT and MEB designed MRI acquisition protocols. KV and JB performed bioinformatic processing. KV analysed the data. JB, GJVB and MLO assisted with data analysis. KV, DB and JPB wrote the paper. All authors significantly contributed to interpreting the results, critically revised the manuscript for important intellectual content and approved the final manuscript.

Competing interests

None of the authors report financial disclosures. The authors declare no competing interests.

References

1. Lawn, J. E. *et al.* Small babies, big risks: global estimates of prevalence and mortality for vulnerable newborns to accelerate change and improve counting. *Lancet* **401**, 1707–1719 (2023).
2. Volpe, J. J. Brain injury in premature infants: a complex amalgam of destructive and developmental disturbances. *Lancet Neurol.* **8**, 110–124 (2009).
3. Wolke, D., Johnson, S. & Mendonça, M. The Life Course Consequences of Very Preterm Birth. *Annu. Rev. Dev. Psychol.* **1**, 69–92 (2019).
4. Counsell, S. J., Arichi, T., Arulkumaran, S. & Rutherford, M. A. Fetal and neonatal neuroimaging. in *Handbook of Clinical Neurology* vol. 162 67–103 (Elsevier B.V., 2019).
5. Boardman, J. P. *et al.* A common neonatal image phenotype predicts adverse neurodevelopmental outcome in children born preterm. *Neuroimage* **52**, 409–414 (2010).
6. Keunen, K. *et al.* Brain volumes at term-equivalent age in preterm infants: Imaging biomarkers for neurodevelopmental outcome through early school age. *J. Pediatr.* **172**, 88–95 (2016).
7. Kline, J. E. *et al.* Early cortical maturation predicts neurodevelopment in very preterm infants. *Arch Dis Child Fetal Neonatal Ed* **105**, 460–465 (2020).
8. Barnett, M. L. *et al.* Exploring the multiple-hit hypothesis of preterm white matter damage using diffusion MRI. *NeuroImage Clin.* **17**, 596–606 (2018).
9. Cryan, J. F. *et al.* The Microbiota-Gut-Brain Axis. *Physiol. Rev.* **99**, 1877–2013 (2019).
10. Spichak, S. *et al.* Mining microbes for mental health: Determining the role of microbial metabolic pathways in human brain health and disease. *Neurosci. Biobehav. Rev.* **125**, 698–761 (2021).
11. Callaghan, B. Nested sensitive periods: how plasticity across the microbiota-gut-brain axis interacts to affect the development of learning and memory. *Curr. Opin. Behav. Sci.* **36**, 55–62 (2020).
12. Cowan, C. S. M., Dinan, T. G. & Cryan, J. F. Annual Research Review: Critical windows – the microbiota–gut–brain axis in neurocognitive development. *J. Child Psychol. Psychiatry* **61**, 353–371 (2019).
13. Vaher, K., Bogaert, D., Richardson, H. & Boardman, J. P. Microbiome-gut-brain axis in brain development, cognition and behavior during infancy and early childhood. *Dev. Rev.* **66**, 101038 (2022).
14. Healy, D. B. *et al.* Clinical implications of preterm infant gut microbiome development. *Nat. Microbiol.* **7**, 22–33 (2022).
15. Henderickx, J. G. E., Zwittink, R. D., Van Lingen, R. A., Knol, J. & Belzer, C. The preterm gut microbiota: An inconspicuous challenge in nutritional neonatal care. *Front. Cell. Infect. Microbiol.* **9**, 85 (2019).
16. Grier, A. *et al.* Impact of prematurity and nutrition on the developing gut microbiome and preterm infant growth. *Microbiome* **5**, 158 (2017).
17. Korpela, K. *et al.* Intestinal microbiota development and gestational age in preterm neonates. *Sci. Rep.* **8**, 2453 (2017).
18. La Rosa, P. S. *et al.* Patterned progression of bacterial populations in the premature infant gut. *Proc Natl Acad Sci* **34**, 12522–12527 (2014).
19. Gasparrini, A. J. *et al.* Persistent metagenomic signatures of early-life hospitalization and antibiotic treatment in the infant gut microbiota and resistome. *Nat. Microbiol. 2019 412* **4**, 2285–2297 (2019).
20. Gregory, K. E. *et al.* Influence of maternal breast milk ingestion on acquisition of the intestinal microbiome in preterm infants. *Microbiome* **4**, 68 (2016).
21. Kumbhare, S. V. *et al.* Source of human milk (mother or donor) is more important than fortifier type (human or bovine) in shaping the preterm infant microbiome. *Cell Reports Med.* **3**, 100712 (2022).
22. Aguilar-Lopez, M., Dinsmoor, A. M., Ho, T. T. B. & Donovan, S. M. A systematic review of the

factors influencing microbial colonization of the preterm infant gut. *Gut Microbes* **13**, 1884514 (2021).

23. Liu, X., Cong, X., Li, G., Maas, K. & Chen, K. Multivariate log-contrast regression with sub-compositional predictors: Testing the association between preterm infants' gut microbiome and neurobehavioral outcomes. *Stat. Med.* **41**, 580–594 (2022).

24. Sun, Z., Xu, W., Cong, X., Li, G. & Chen, K. Log-contrast regression with functional compositional predictors: Linking preterm infants' gut microbiome trajectories to neurobehavioral outcome. *Ann. Appl. Stat.* **14**, 1535–1556 (2020).

25. Beghetti, I. *et al.* Early-life gut microbiota and neurodevelopment in preterm infants: any role for Bifidobacterium? *Eur. J. Pediatr.* **1**, (2021).

26. Rozé, J.-C. *et al.* Assessment of Neonatal Intensive Care Unit Practices and Preterm Newborn Gut Microbiota and 2-Year Neurodevelopmental Outcomes. *JAMA Netw. Open* **3**, Article e2018119 (2020).

27. Sarkar, A. *et al.* Relationships of the very low birth weight infant microbiome with neurodevelopment at 2 and 4 years of age. *Dev. Psychobiol.* **64**, (2022).

28. Seki, D. *et al.* Aberrant gut-microbiota-immune-brain axis development in premature neonates with brain damage. *Cell Host Microbe* **29**, 1–15 (2021).

29. Boardman, J. P. *et al.* Impact of preterm birth on brain development and long-term outcome: protocol for a cohort study in Scotland. *BMJ Open* **10**, 35854 (2020).

30. Vieira-Silva, S. *et al.* Species–function relationships shape ecological properties of the human gut microbiome. *Nat. Microbiol. 2016 18* **1**, 1–8 (2016).

31. Darzi, Y., Falony, G., Vieira-Silva, S. & Raes, J. Towards biome-specific analysis of meta-omics data. *ISME J. 2016 105* **10**, 1025–1028 (2015).

32. Cong, X. *et al.* Gut Microbiome Developmental Patterns in Early Life of Preterm Infants: Impacts of Feeding and Gender. *PLoS One* **11**, e0152751 (2016).

33. Beck, L. C. *et al.* Strain-specific impacts of probiotics are a significant driver of gut microbiome development in very preterm infants. *Nat. Microbiol.* **7**, 1525–1535 (2022).

34. Garfinkle, J. *et al.* Trends in sex-specific differences in outcomes in extreme preterms: progress or natural barriers? *Arch. Dis. Child. - Fetal Neonatal Ed.* **105**, 158–163 (2020).

35. Mallick, H. *et al.* Multivariable Association Discovery in Population-scale Meta-omics Studies. *PLOS Comput. Biol.* **17**, e1009442 (2021).

36. Valles-Colomer, M. *et al.* The neuroactive potential of the human gut microbiota in quality of life and depression. *Nat. Microbiol.* **4**, 623–632 (2019).

37. Rao, C. *et al.* Multi-kingdom ecological drivers of microbiota assembly in preterm infants. *Nature* **591**, 633–638 (2021).

38. Klopp, J. *et al.* Meconium Microbiome of Very Preterm Infants across Germany. *mSphere* **7**, (2022).

39. Enav, H., Bäckhed, F. & Ley, R. E. The developing infant gut microbiome: A strain-level view. *Cell Host Microbe* **30**, 627–638 (2022).

40. Ardissone, A. N. *et al.* Meconium microbiome analysis identifies bacteria correlated with premature birth. *PLoS One* **9**, e90784 (2014).

41. Klopp, J. *et al.* Meconium Microbiome of Very Preterm Infants across Germany. *mSphere* **7**, (2022).

42. Bäckhed, F. *et al.* Dynamics and stabilization of the human gut microbiome during the first year of life. *Cell Host Microbe* **17**, 690–703 (2015).

43. Reyman, M. *et al.* Impact of delivery mode-associated gut microbiota dynamics on health in the first year of life. *Nat. Commun.* **10**, Article 4997 (2019).

44. Valeri, F. & Endres, K. How biological sex of the host shapes its gut microbiota. *Front. Neuroendocrinol.* **61**, 100912 (2021).

45. Nagpal, R. *et al.* Evolution of gut Bifidobacterium population in healthy Japanese infants over the first three years of life: a quantitative assessment. *Sci. Rep.* **7**, 10097 (2017).

46. Cong, X. *et al.* Gut Microbiome Developmental Patterns in Early Life of Preterm Infants: Impacts of Feeding and Gender. *PLoS One* **11**, e0152751 (2016).

47. Reyman, M. *et al.* Effects of early-life antibiotics on the developing infant gut microbiome and resistome: a randomized trial. *Nat. Commun.* **13**, 893 (2022).

48. Carlson, A. L. *et al.* Infant gut microbiome composition is associated with non-social fear behavior in a pilot study. *Nat. Commun.* **12**, Article 3294 (2021).

49. Luczynski, P. *et al.* Adult microbiota-deficient mice have distinct dendritic morphological changes: differential effects in the amygdala and hippocampus. *Eur. J. Neurosci.* **44**, 2654–2666 (2016).

50. Loh, W. Y. *et al.* Neonatal basal ganglia and thalamic volumes: very preterm birth and 7-year neurodevelopmental outcomes. *Pediatr. Res.* **82**, 970–978 (2017).

51. Boardman, J. P. *et al.* Abnormal deep grey matter development following preterm birth detected using deformation-based morphometry. *Neuroimage* **32**, 70–78 (2006).

52. Ball, G. *et al.* The Effect of Preterm Birth on Thalamic and Cortical Development. *Cereb. Cortex* **22**, 1016–1024 (2012).

53. Dimitrova, R. *et al.* Preterm birth alters the development of cortical microstructure and morphology at term-equivalent age. *Neuroimage* **243**, 118488 (2021).

54. Sordillo, J. E. *et al.* Association of the Infant Gut Microbiome With Early Childhood Neurodevelopmental Outcomes: An Ancillary Study to the VDAART Randomized Clinical Trial. *JAMA Netw. open* **2**, Article e190905 (2019).

55. Bansal, T., Alaniz, R. C., Wood, T. K. & Jayaraman, A. The bacterial signal indole increases epithelial-cell tight-junction resistance and attenuates indicators of inflammation. *Proc. Natl. Acad. Sci. U. S. A.* **107**, 228–233 (2010).

56. Rothhammer, V. *et al.* Type I interferons and microbial metabolites of tryptophan modulate astrocyte activity and central nervous system inflammation via the aryl hydrocarbon receptor. *Nat. Med. 2016 226* **22**, 586–597 (2016).

57. Silva, Y. P., Bernardi, A. & Frozza, R. L. The Role of Short-Chain Fatty Acids From Gut Microbiota in Gut-Brain Communication. *Front. Endocrinol. (Lausanne).* **11**, 1–14 (2020).

58. Hoyles, L. *et al.* Microbiome–host systems interactions: Protective effects of propionate upon the blood–brain barrier. *Microbiome* **6**, 1–13 (2018).

59. Sharif, S., Meader, N., Oddie, S. J., Rojas-Reyes, M. X. & McGuire, W. Probiotics to prevent necrotising enterocolitis in very preterm or very low birth weight infants. *Cochrane Database Syst. Rev.* **2023**, (2023).

60. Nearing, J. T., Comeau, A. M. & Langille, M. G. I. Identifying biases and their potential solutions in human microbiome studies. *Microbiome* **9**, 113 (2021).

61. Carlson, A. L. *et al.* Infant Gut Microbiome Associated With Cognitive Development. *Biol. Psychiatry* **83**, 148–159 (2018).

62. Gao, W. *et al.* Gut microbiome and brain functional connectivity in infants-a preliminary study focusing on the amygdala. *Psychopharmacology (Berl).* **236**, 1641–1651 (2019).

63. Kelsey, C. M. *et al.* Gut microbiota composition is associated with newborn functional brain connectivity and behavioral temperament. *Brain. Behav. Immun.* **91**, 472–486 (2021).

64. Schoch, S. F. *et al.* From Alpha Diversity to Zzz: Interactions among sleep, the brain, and gut microbiota in the first year of life. *Prog. Neurobiol.* **209**, 102208 (2022).

65. Hunter, S. *et al.* Babies, bugs and brains: How the early microbiome associates with infant brain and behavior development. *PLoS One* **18**, e0288689 (2023).

66. Lu, J. *et al.* Effects of Intestinal Microbiota on Brain Development in Humanized Gnotobiotic Mice OPEN. *Sci. Data* **8**, Article 5443 (2018).

67. Lu, J. *et al.* Microbiota from Preterm Infants Who Develop Necrotizing Enterocolitis Drives the

Neurodevelopment Impairment in a Humanized Mouse Model. *Microorg. 2023, Vol. 11, Page 1131* **11**, 1131 (2023).

68. Biesbroek, G. *et al.* Deep sequencing analyses of low density microbial communities: Working at the boundary of accurate microbiota detection. *PLoS One* **7**, e32942 (2012).

69. Bogaert, D. *et al.* Variability and Diversity of Nasopharyngeal Microbiota in Children: A Metagenomic Analysis. *PLoS One* **6**, e17035 (2011).

70. Bogaert, D. *et al.* Mother-to-infant microbiota transmission and infant microbiota development across multiple body sites. *Cell Host Microbe* **31**, 447-460.e6 (2023).

71. Caporaso, J. G. *et al.* Global patterns of 16S rRNA diversity at a depth of millions of sequences per sample. *Proc. Natl. Acad. Sci. U. S. A.* **108**, 4516–4522 (2011).

72. R Core Team. R: A language and environment for statistical computing. R Foundation for Statistical Computing. https://www.r-project.org/ (2022).

73. de Steenhuijsen Piters, W. A. A. *et al.* Early-life viral infections are associated with disadvantageous immune and microbiota profiles and recurrent respiratory infections. *Nat. Microbiol. 2022 72* **7**, 224–237 (2022).

74. Callahan, B. J. *et al.* DADA2: High-resolution sample inference from Illumina amplicon data. *Nat. Methods 2016 137* **13**, 581–583 (2016).

75. Davis, N. M., Proctor, Di. M., Holmes, S. P., Relman, D. A. & Callahan, B. J. Simple statistical identification and removal of contaminant sequences in marker-gene and metagenomics data. *Microbiome* **6**, 226 (2018).

76. Subramanian, S. *et al.* Persistent gut microbiota immaturity in malnourished Bangladeshi children. *Nature* **510**, 417–421 (2014).

77. Martin, M. Cutadapt removes adapter sequences from high-throughput sequencing reads. *EMBnet.journal* **17**, 10–12 (2011).

78. Langmead, B., Wilks, C., Antonescu, V. & Charles, R. Scaling read aligners to hundreds of threads on general-purpose processors. *Bioinformatics* **35**, 421–432 (2019).

79. Beghini, F. *et al.* Integrating taxonomic, functional, and strain-level profiling of diverse microbial communities with biobakery 3. *Elife* **10**, (2021).

80. Vaher, K. *et al.* General factors of white matter microstructure from DTI and NODDI in the developing brain. *Neuroimage* **254**, 119169 (2022).

81. Makropoulos, A. *et al.* The developing human connectome project: A minimal processing pipeline for neonatal cortical surface reconstruction. *Neuroimage* **173**, 88–112 (2018).

82. Greve, D. N. & Fischl, B. Accurate and robust brain image alignment using boundary-based registration. *Neuroimage* **48**, 63–72 (2009).

83. Guerrero, J. M. *et al.* Optimizing the intrinsic parallel diffusivity in NODDI: An extensive empirical evaluation. *PLoS One* **14**, e0217118 (2019).

84. Zhang, H., Schneider, T., Wheeler-Kingshott, C. A. & Alexander, D. C. NODDI: Practical in vivo neurite orientation dispersion and density imaging of the human brain. *Neuroimage* **61**, 1000–1016 (2012).

85. Avants, B. B., Epstein, C. L., Grossman, M. & Gee, J. C. Symmetric diffeomorphic image registration with cross-correlation: Evaluating automated labeling of elderly and neurodegenerative brain. *Med. Image Anal.* **12**, 26–41 (2008).

86. Wickham, H. ggplot2: Elegant Graphics for Data Analysis Second Edition. https://ggplot2.tidyverse.org (2016).

87. Kassambara, A. Package ‘ggpubr’. https://cran.r-project.org/web/packages/ggpubr/index.html (2020).

88. Wilke, C. O. Cowplot package. (2020).

89. Benjamini, Y. & Hochberg, Y. Controlling the False Discovery Rate: A Practical and Powerful Approach to Multiple Testing. *J. R. Stat. Soc. Ser. B* **57**, 289–300 (1995).

90. Bray, J. R. & Curtis, J. T. An Ordination of the Upland Forest Communities of Southern Wisconsin. *Ecol. Monogr.* **27**, 325–349 (1957).

91. Oksanen, J. *et al.* vegan: Community Ecology Package. R package version 2.6-2. (2019) doi:https://github.com/vegandevs/vegan/.

92. Paradis, E. & Schliep, K. ape 5.0: an environment for modern phylogenetics and evolutionary analyses in R. *Bioinformatics* **35**, 526–528 (2019).

93. Cailliez, F. The analytical solution of the additive constant problem. *Psychom. 1983 482* **48**, 305–308 (1983).

94. McMurdie, P. J. & Holmes, S. phyloseq: An R Package for Reproducible Interactive Analysis and Graphics of Microbiome Census Data. *PLoS One* **8**, e61217 (2013).

95. Kuznetsova, A., Brockhoff, P. B. & Christensen, R. H. B. lmerTest Package: Tests in Linear Mixed Effects Models. *J. Stat. Softw.* **82**, 1–26 (2017).

96. Lenth, R. V. emmeans: Estimated Marginal Means, aka Least-Squares Means. R package version 1.8.0. (2022) doi:10.1080/00031305.1980.10483031.

97. Aatsinki, A. K. *et al.* Gut microbiota composition is associated with temperament traits in infants. *Brain. Behav. Immun.* **80**, 849–858 (2019).

98. Mirzayi, C. *et al.* Reporting guidelines for human microbiome research: the STORMS checklist. *Nat. Med. 2021 2711* **27**, 1885–1892 (2021).